

Research article

Origin and evolution of the Neoproterozoic Dengganping Granitic Complex in the western margin of the Yangtze Block, SW China: Implications for breakup of Rodina Supercontinent

Hao Zou ^{a,b,*}, Leon Bagas ^{a,c,d,*}, Xin-Yu Li ^{e,f}, Hang Liu ^{a,g}, Xiu-Wei Jiang ^b, Yang Li ^{a,g}^a Key Laboratory of Tectonic Controls on Mineralisation and Hydrocarbon Accumulation of Ministry of Land and Resources, Chengdu University of Technology, Sichuan 610059, China^b State Key Laboratory of Lithospheric Evolution, Institute of Geology and Geophysics, Chinese Academy of Sciences, Beijing 100029, China^c Centre of Exploration Targeting, The University of Western Australia, 35 Stirling Highway, Crawley, WA 6009, Australia^d Xi'an Center of China Geological Survey, 438 Youyi Road, Xi'an 710054, China^e State Key Laboratory of Environmental Geochemistry, Institute of Geochemistry, Chinese Academy of Sciences, Guiyang 550081, China^f The University of Chinese Academy of Sciences, Beijing 100049, China^g State Key Laboratory for Mineral Deposits Research, Nanjing University, Nanjing 210023, China

ARTICLE INFO

Article history:

Received 28 March 2020

Received in revised form 13 May 2020

Accepted 22 May 2020

Available online 2 June 2020

Keywords:

Rodinia Supercontinent

Dengganping Complex

Break-up

U-Pb zircon age

Hf-O-Nd isotopes

ABSTRACT

A better understanding of the origin and evolution of widespread Neoproterozoic granites along the western margin of the Yangtze Block is important in locating the position of South China within the Rodinia Supercontinent, and the mechanism by which the supercontinent was fragmented. Published and our new detailed geochronological and geochemical data from the Dengganping Complex show that it formed during an extended magmatic event during the Neoproterozoic. This was during the emplacement of a fractionated ca. 815 Ma syenogranite, which was followed by partial melting during ca. 740 Ma and the emplacement of a biotite monzogranite. The geochemistry of the syenogranite indicates it is: (1) a peraluminous high-K type of granite; (2) calc-alkaline; (3) fractionated; (4) enriched in Th, U, Zr, Hf and LREE (LREE/HREE values of 5.3–9); (5) depleted in Nb and Sr; (6) has a negative Eu anomaly ($\delta\text{Eu} = 0.3\text{--}0.5$); (7) has whole rock $\epsilon_{\text{Nd}}(t)$ value of -0.7 to $+0.5$; (8) has zircon $\epsilon_{\text{Hf}}(t)$ value of -1.7 to $+5.2$; and (9) has zircon ^{18}O values ranging from 5.13 to 7.38‰. These characteristics are indicative of a source derived from the partial melting of crustal material. The biotite monzogranite is: (i) peraluminous calc-alkaline to high-K calc-alkaline; (ii) enriched in LREE (LREE/HREE = 9.9–14.6), Rb, Ba, Th and U; (iii) depleted in Nb and Ta; (iv) has weak negative δEu and δCe anomalies; (v) has whole rock $\epsilon_{\text{Nd}}(t)$ value of between -3.2 and -1.8 ; has relatively high positive zircon $\epsilon_{\text{Hf}}(t)$ values of $+4.1$ to $+13$; and has zircon ^{18}O values ranging from 3.44 to 6.75‰. These features are indicative of partial melting of a juvenile mafic crust that might have experienced a high-temperature water-rock interaction. By comparing the geochronology of Neoproterozoic magmatic rocks along the faulted western margin of the Yangtze Block, it is suggested that the region was part of the Rodinia Supercontinent when it started to breakup during widespread rifting between ca. 825 and 710 Ma. We believe the fault zone formed in response to an opening ocean was induced by the presence of a mantle plume during this period.

© 2020 Elsevier B.V. All rights reserved.

1. Introduction

The Rodinia Supercontinent formed during the convergence of continental blocks in the Meso- to Neoproterozoic and broke up in the Neoproterozoic (Dalziel, 1991; Hoffman, 1991; McMenamin and McMenamin, 1990; Moores, 1991; Valentine and Moores, 1970). The new blocks formed during the fragmentation of the supercontinent

were the loci of the most rapid increase in animal and botanic diversity in Earth's history, and the deposition of many mineral deposits during the Phanerozoic.

The position of present-day continents within the Rodinia Supercontinent is uncertain, with well-known models such as those proposed by Hoffman (1991), Li et al. (1995), Li et al. (1996), and Torsvik (2003). In addition, there is a great deal of uncertainty about the detailed location of individual plates involved in the convergence and fragmentation of the supercontinent (Cawood and Pisarevsky, 2017; Condé, 2001; Li et al., 2008).

Studies of the convergence of the Rodinia Supercontinent has historically focused on the Greenville area in eastern USA, whereas studies on

* Corresponding authors at: Key Laboratory of Tectonic Controls on Mineralisation and Hydrocarbon Accumulation of Ministry of Land and Resources, Chengdu University of Technology, Sichuan 610059, China.

E-mail addresses: zouhao21@gmail.com (H. Zou), Leon.Bagas@uwa.edu.au (L. Bagas).

its fragmentation are diverse regions of the Earth in areas local to the authors. The northwestern margin of the Yangtze Block in China is an example that records its separation from the supercontinent during ca. 825–710 Ma (Li et al., 2002b; Liu et al., 2009a, 2009b; Zhang et al., 2008). This is when a large number of Neoproterozoic intermediate to felsic plutons were emplaced in the Pengguan, Qiaoziding, Xuelongbao, Kangding, and Panzhihua complexes that have been multiply deformed and metamorphosed during the Phanerozoic (SPBGMR, 1991; Lin and Ma, 1995; Ma et al., 1996; Chen et al., 2004; Zhao et al., 2006, 2011; Zhou et al., 2006; Li et al., 2006; Zhang et al., 2008; Liu, 2013).

The theories posited for the tectonic setting of the Neoproterozoic magmatism along the western margin of the Yangtze Block are:

- (1) The development of a continental rift formed by major upwelling mantle plume (Huang et al., 2008; Li et al., 2002a, 2002b; Li et al., 2003a, 2003b, 2003c; Li and Powell, 2001; Wingate et al., 1998; Zhu et al., 2004, 2008).
- (2) An oceanic subduction or volcanic-arc and both sourced from a mixed mantle and lower-crustal source (Chen et al., 2004; Du et al., 2007; Geng et al., 2007; Liu et al., 2009a; Mu et al., 2003; Zhang et al., 2008; Zhao et al., 2006; Zhou et al., 2002, 2006).

The clarity of these options has been made difficult following the consequent deformation and metamorphism due to the convergence of the North China and Yangtze blocks along the Central China Orogen,

and the convergence of the Yangtze Block with the Indian continental plate (Fig. 1).

This contribution presents constraints on the origin and tectonic setting of the Dengganping Complex along the western margin of the Yangtze Block in South China. The results of the new magmatic zircon U–Pb geochronology, Hf–O isotope and whole rock Nd isotope and geochemistry provide a better understanding of the tectonic setting for the Neoproterozoic magmatic rocks in the study area, which are placed in context with the breakup of the Rodinia Supercontinent.

2. Geology

2.1. Regional geology

The Dengganping Complex consists of syenogranite with lesser gabbroic, dioritic, tonalitic and granodioritic orthogneiss intruded by monzogranite. The complex is located between the Baoxing Complex to the southwest and Pengguan Complex in the western part of the Yangtze Block (Figs. 1 and 2; Liu et al., 2009c). The complexes are located near the southeastern margin of the Qinghai-Tibet Plateau and Longmenshan Fault Zone (Figs. 1 and 2). The fault zone includes NE-trending thrusts with apparent movement toward the SE, NNE- to NE-trending folds, and klippe structures (Figs. 1 and 2). The zone separates Triassic units in the Songpan-Ganzi Orogen that are thrust onto

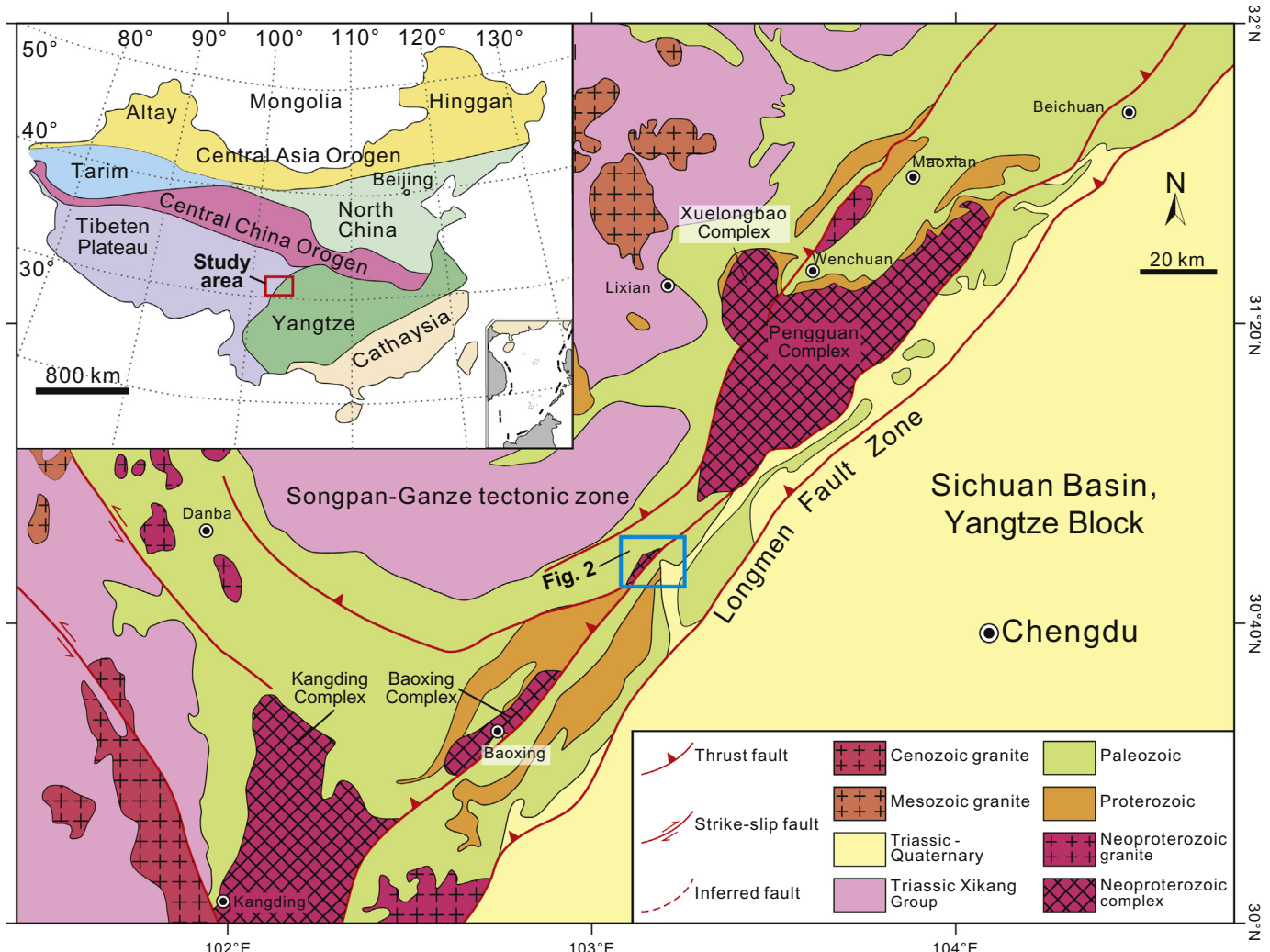


Fig. 1. Simplified geological map of the western margin of the Yangtze Block (modified after Yan et al., 2011).

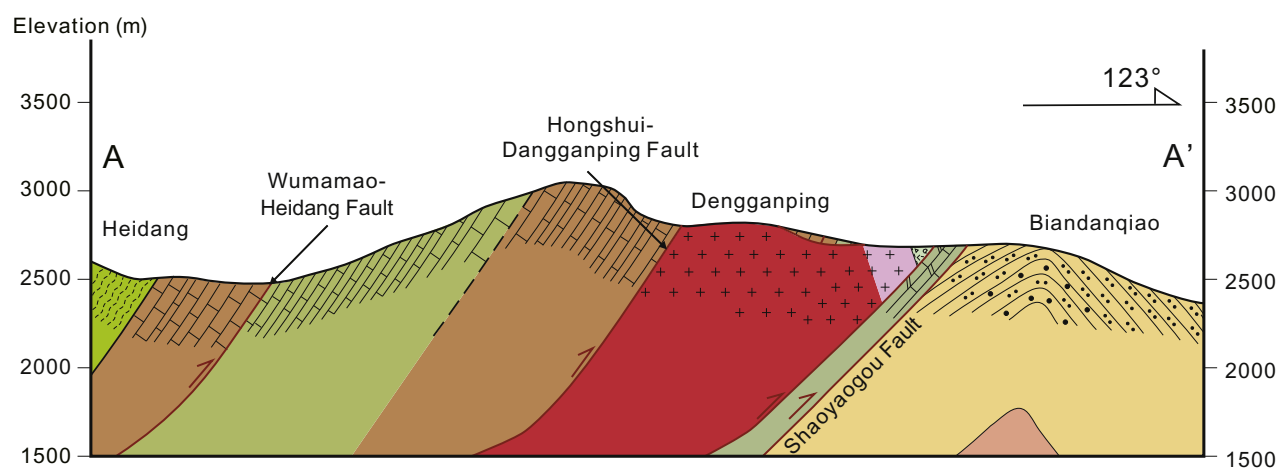
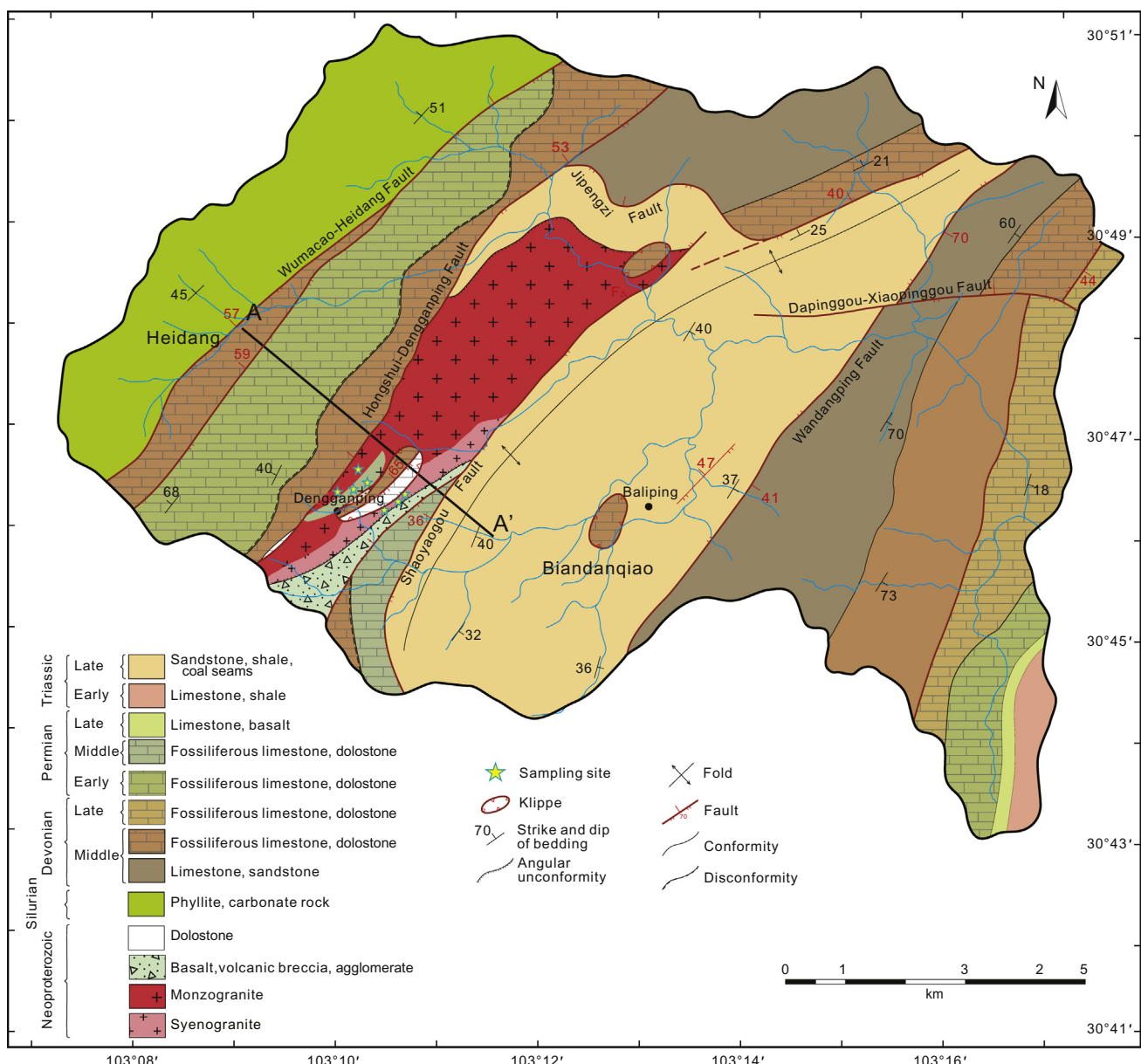


Fig. 2. Geological map of Dengganping Complex and adjacent areas.

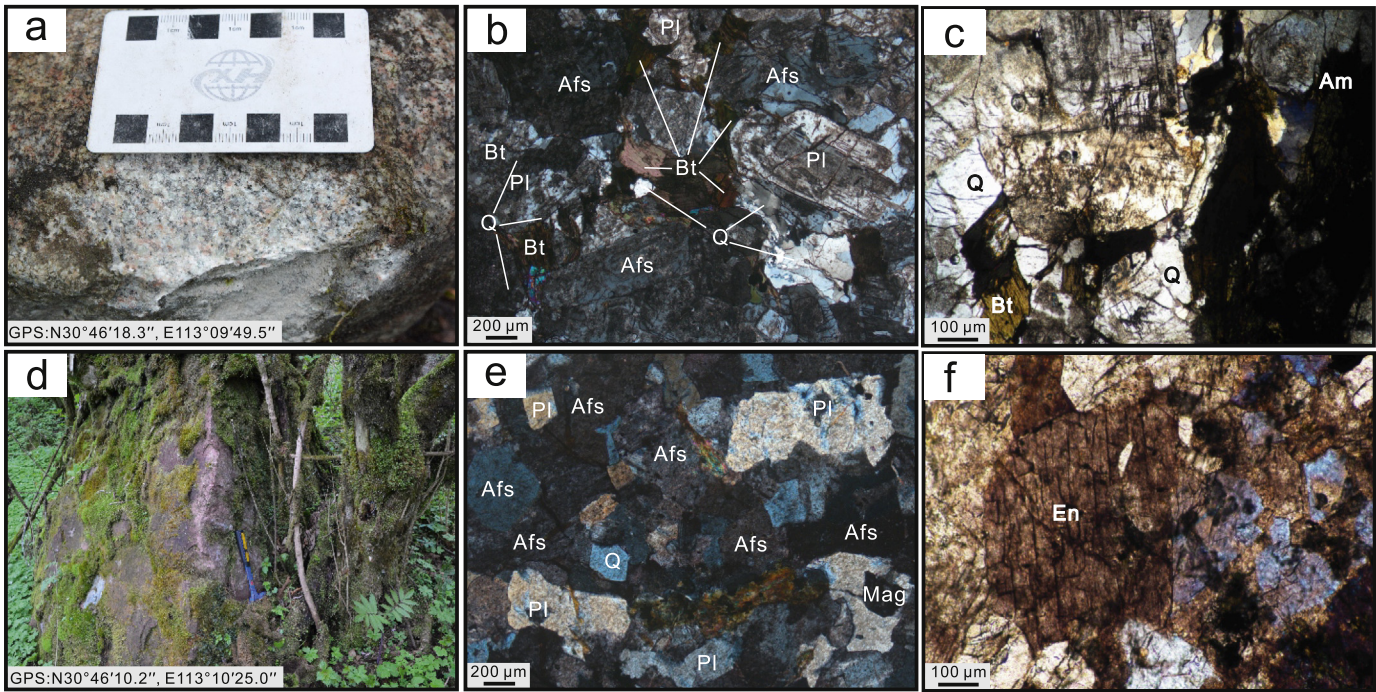


Fig. 3. Photographs of the Dengganping Complex showing: (a) field photograph of the biotite monzogranite; (b) cross-polar photomicrograph of the biotite monzogranite; (c) field photograph of the biotite monzogranite; and (d) cross-polar photomicrograph of the syenogranite. Abbreviation: Afs—alkali feldspar; Pl—plagioclase; Q—quartz; Am—amphibole; Mag—magnetite; En—enstatite.

Neoproterozoic to Paleozoic units in the Yangtze Block to the east (Fig. 1; SPBGMR, 1991). The region around Dengganping is affected by Mesozoic orogenies characterised by folds and faults that are broadly synchronous with magmatic events. The orogenic events were included in the “Yanshanian Uplift” (e.g. Burchfiel et al., 1995; Huang and Chen, 1987; Nie et al., 1994; She et al., 2006).

Rapid Mesozoic uplift of the Tibetan Plateau resulted in the exposure of Neoproterozoic units along the Longmenshan Fault Zone, which are unconformably overlain by Late Neoproterozoic (Ediacaran) and Paleozoic supracrustal units along the western margin of the Yangtze Block (He et al., 1988). This includes the ca. 869–699 Ma Pengguan, ca. 825 Ma Baoxing, ca. 750 Ma Xuelongbao, and ca. 773–721 Ma Kangding complexes (Fig. 1; Ma et al., 1996; Li et al., 2002b, 2006; Chen et al., 2004; Zhou et al., 2006; Zhao et al., 2006, 2011; Zhang et al., 2008; Liu, 2013).

The Wandangping, Shaoyaogou, Hongshui-Dengganping, Wumacao-Heidang, Dapinggou-Xiaopinggou, and Jipengzi faults are present in the study area (Fig. 2). The Jipengzi Fault is the oldest being cut by the NE-trending Hongshui-Dengganping Fault. The relatively younger NE-trend Shaoyaogou, Hongshui-Dengganping and Wumacao-Heidang faults dip moderately to the NW (Fig. 2). The Wandangping Fault is different trending NNE and dipping 40°–70° SE, and the Dapinggou-Xiaopinggou Fault is relatively late trending eastward, dipping north and crosscuts the Wandangping Fault.

A refolded NE-trending (F_1) anticline with an axial plane dipping ~85° NW is present in the central part of the study area and has affected

Late Triassic sandstone, shale, and coal seams. The anticline has been refolded by a close fold (F_2) with an axial trace trending SE. This indicates that the main structures in the area are related to E-W to NW-SE orientated compression and the refolding is indicative of compression orientated NE-SW (Fig. 2).

2.2. Petrology of the granitic phases in the Dengganping Complex

The Neoproterozoic Dengganping Complex consists of biotite monzogranite (samples Y0212, 0402, 0405, 0407, 0302, 0403, 0408, 0418) and syenogranite (samples Y0412, 0414, 0415, 0416, 0417, 0419; Fig. 3; Table 1; ‘biotite’ is added to the name of the granites when biotite is >5 wt%). The biotite monzogranite contains medium-to fine-grained, is grey to white, and consists of plagioclase (30–40 wt %), K-feldspar (20–30 wt%), quartz (20–25 wt%), biotite (5–10 wt%), opaques minerals (<1 wt%), and trace amounts of zircon, apatite, and magnetite. Metasomatised K-feldspar and plagioclase altered to albite and sericite forming irregular aggregates with an indistinct polysynthetic twinning, and the presence of the intergrowth of quartz in plagioclase forming a vermicular texture.

The syenogranite is medium- to fine-grained, equigranular, pale red in colour, and consists of K-feldspar (40–50 wt%), plagioclase (10–25 wt %) partially altered to albite and sericite, quartz (20–25 wt%), biotite (<1 wt%), opaques minerals (<1 wt%), and trace amounts of magnetite, zircon and apatite. The K-feldspar is microcline, subhedral measuring ≤5 mm long, and has cross-hatched twinning (Fig. 2e, f). The plagioclase is

Table 1
Composition of the granitic phases in the Dengganping Complex.

Phase	Texture and grain size	Main minerals	Accessory minerals
Biotite monzogranite (Fig. 3a, b)	Grey to pale pink, massive, medium- to fine-grained, idiomorphic or hypidiomorphic	Red K-feldspar (20–30 wt%) ≤6 mm wide; grey plagioclase (30–40 wt%) ≤7 mm long; smoky quartz (20–25 wt%); biotite (5–10 wt%)	Zircon, apatite, magnetite, monazite, allanite, fluorite, and minor rutile
Syenogranite (Fig. 3c, d)	Red, massive, medium- to fine-grained, idiomorphic or hypidiomorphic	Hypidiomorphic and granular, perthitic K-feldspar (40–50 wt% ≤5 mm long); grey plagioclase partially altered to sericite and albite (10–25 wt%); quartz (20–25 wt%, ≤2 mm wide)	Magnetite, zircon, apatite, and minor amounts of vermiculite, monazite, allanite and fluorite

andesine, 2–5 mm long, and has oscillatory zoning and is variable altered to sericite. The quartz is ≤2 mm across, granular and commonly mixed with K-feldspar and plagioclase.

3. Sampling and analytical methods

Fourteen representative samples were collected from outcrops in the Dengganping area (located 113°09'50" E to 113°10'25" E and 30°46'10" N to 30°46'18" N) for various analyses. Four samples (Y0407, Y0408, Y0412, and Y0414) were analysed for SIMS U—Pb zircon dated, in-situ zircon Hf—O isotopes, LA-ICP-MS Zircon U—Pb geochronology, fourteen samples of fresh granites analysed for major and trace elements, and four samples analysed for whole-rock Nd isotopes. Detailed experimental procedures and data are presented in Supplementary material 1 and 2.

4. Analytical results

4.1. U—Pb zircon dating

The secondary ion mass spectrometry (SIMS) U—Pb zircon analyses and Laser Ablation-Inductively Coupled Plasma-Mass Spectrometry (LA-ICP-MS) U—Pb zircon dating of samples from the two granitic phases in the Dengganping Complex are presented in Table S1.

Biotite monzogranite sample Y0407 contains euhedral, granular, and elongate and columnar zircons, and have clear oscillatory zoning on CL images characteristic of magmatic zircons (Fig. 4a; Rubatto, 2002). Twenty U—Pb analyses on 20 zircon grains were completed using the SIMS. The zircons from sample Y0407 yielded an intercept age of 751 ± 14 Ma, excluding eight discordant analyses interpreted as due to Pb-loss, the remaining 12 analyses define a concordia age of 747 ± 6 Ma (Fig. 5a). This age is taken as the best estimate of the granite's crystallisation age. Nineteen spots were measured using the LA-ICP-MS on 19 zircon grains yielding similar $^{206}\text{Pb}/^{238}\text{U}$ dates ranging from 748 to 741 Ma, and all plot on or near the U—Pb age Concordia curve with a weighted mean age of 743 ± 4 Ma (Fig. 5b).

Zircons from the biotite monzogranite sample Y0408 are euhedral, granular, elongate, or columnar (Fig. 4b). Twenty U—Pb analyses were conducted using the SIMS on 20 grains with clear oscillatory zoning characteristic of a magmatic origin. The zircons from the sample yielded an intercept age of 751 ± 14 Ma, excluding eight discordant analyses interpreted as due to Pb-loss, the remaining 8 analyses define with a weighted average of 742 ± 25 Ma (Fig. 5c). Twelve spots were measured using the LA-ICP-MS on 12 zircon grains. The zircons yield $^{206}\text{Pb}/^{238}\text{U}$ dates of 749–741 Ma, and plot on or near the U—Pb age Concordia curve (Fig. 5d). The analyses yield a weighted mean age of 742 ± 5 Ma, which is interpreted as the emplacement age of the biotite monzogranite.

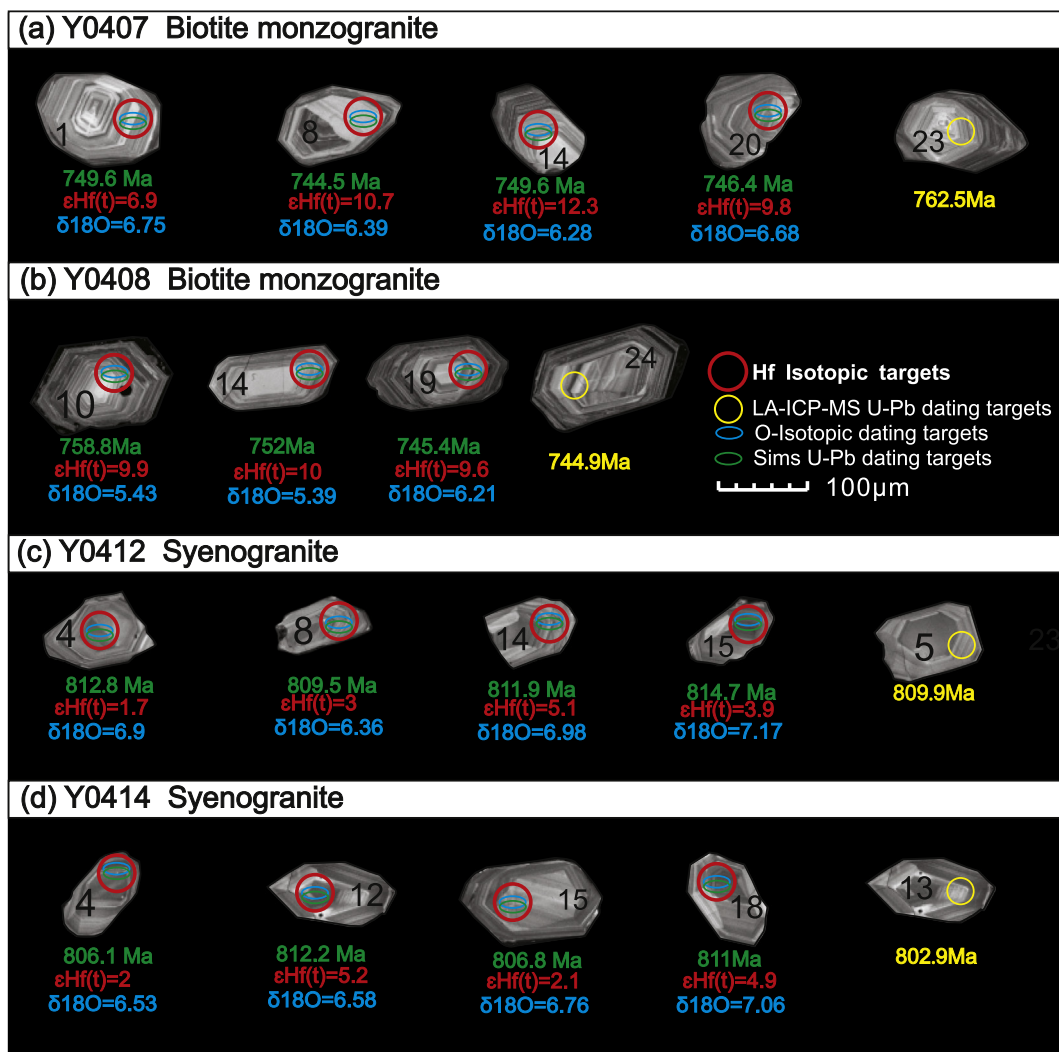


Fig. 4. Zircon CL images with U—Pb ages for: (a, b) Biotite monzogranite; and (c, d) Syenogranite.

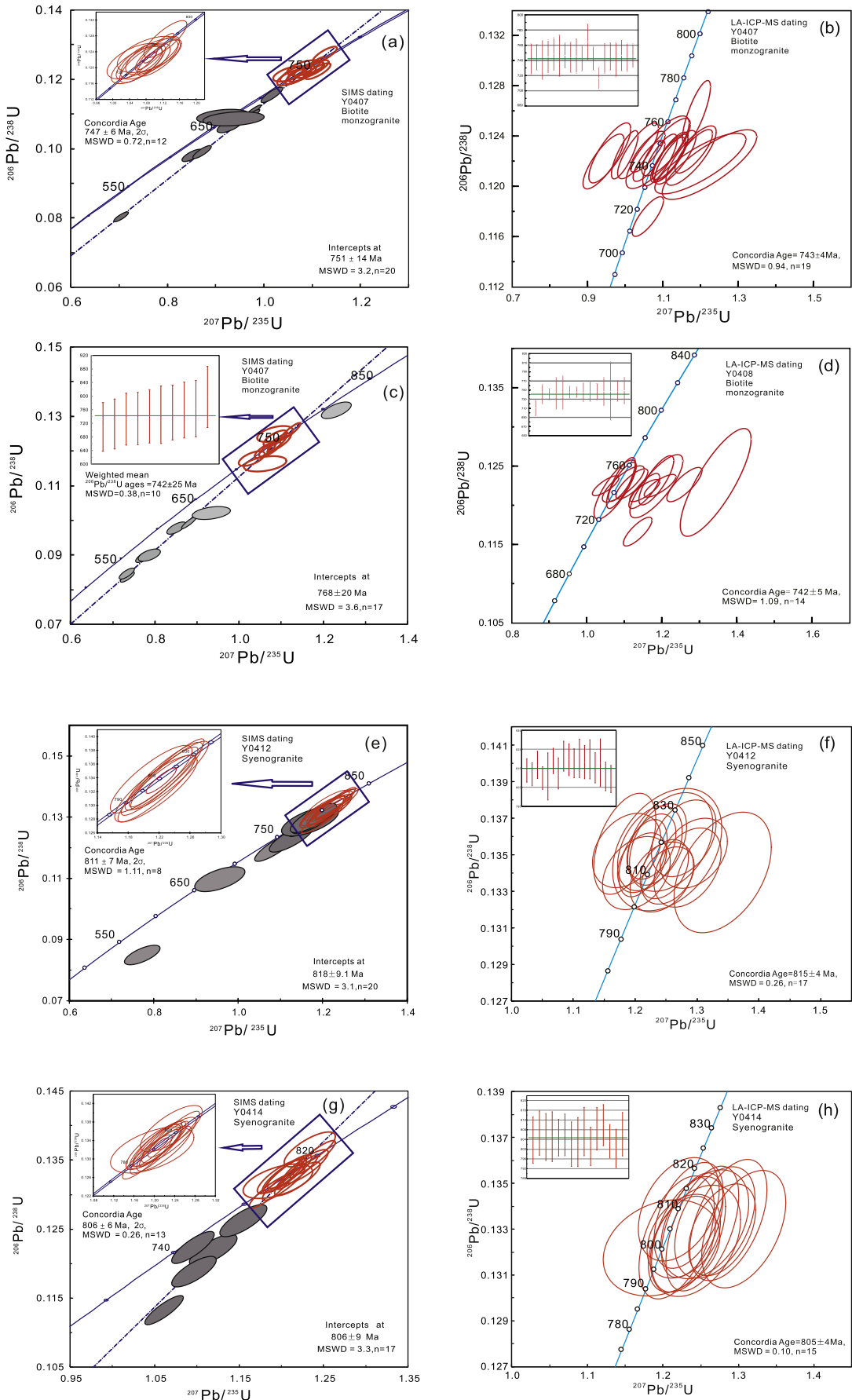


Fig. 5. Concordia diagrams of zircon U–Pb data for: (a-d) Biotite monzogranite; and (e-h) Syenogranite.

Zircons from syenogranite samples Y0412 and Y0414 are euhedral, granular, elongate, or columnar (Fig. 4c, d). The CL images of the zircons dated from the two samples have oscillatory zoning characteristic of a magmatic origin (Rubatto, 2002). Twenty U—Pb analyses were completed using the SIMS on 20 grains. The zircons from sample Y0412 yielded an intercept age of 818 ± 9 Ma, and eight analyses define a concordia age of 811 ± 7 Ma (Fig. 5e). Zircons from sample Y0412 yielded $^{206}\text{Pb}/^{238}\text{U}$ LA-ICP-MS dates ranging from 819 to 811 Ma, which plot on or near the U—Pb age Concordia curve (Fig. 5f). The weighted mean age is 815 ± 4 Ma. Twenty U—Pb analyses were conducted using the SIMS on 20 grains from sample Y0414 yielding an intercept age of 813 ± 6 Ma, 13 analyses define a concordia age of 806 ± 6 Ma (Fig. 5g), and 15 zircons yielded $^{206}\text{Pb}/^{238}\text{U}$ dates ranging from 807 to 802 Ma, which plot on or near the U—Pb age Concordia curve. The weighted mean age is 805 ± 4 Ma (Fig. 5h).

4.2. Zircon trace elements

Zircon trace elements are sensitive monitors of the composition and temperature of their parental magma (e.g. Belousova et al., 2006; Grimes et al., 2015; Yuan et al., 2018). The trace element content of zircons from the samples are listed in Tables S2 and S3. The biotite monzogranite sample Y0407 has a fractionated chondrite-normalised REE pattern indicated by positive Ce and negative Eu anomalies (Table S3; Fig. 6a; Hoskin and Schaltegger, 2003; Whitehouse and Platt, 2003). The zircons' Th/U ratios are 0.3–1.02, Nb/Yb are 0.002–0.005, and U/Yb are 0.21–0.62. The biotite monzogranite sample

Y0408 also has a fractionated chondrite-normalised REE pattern indicated by positive Ce and negative Eu anomalies (Table S3; Fig. 6b; Hoskin and Schaltegger, 2003; Whitehouse and Platt, 2003). The zircons' Th/U ratios are 0.44–0.97, Nb/Yb are 0.002–0.006, and U/Yb are 0.21–1.51.

The trace element content of zircons from syenogranite sample Y0412 have negative Ce and Eu anomalies (Table S3; Fig. 6c). The zircons' Th/U ratios are 0.8–1.18, Nb/Yb ratios are 0.002–0.01, and U/Yb ratios are 0.29–0.62 (Fig. 6). The trace element content of the zircons from syenogranite sample Y0414 have both positive and negative Ce and negative Eu anomalies (Table S3; Fig. 6d). The zircons' Th/U ratios are 0.8–1.52, Nb/Yb ratios are 0.002–0.01, and U/Yb ratios are 0.32–0.8 (Table S3, Fig. 6).

4.3. Zircon Lu—Hf isotopes

The areas around zircon spots with SIMS U—Pb dates were analysed for their Lu—Hf isotopic composition aiming to determine the source of magmatism in the Dengganping Complex (Fig. 5). The Lu—Hf isotope analyses are presented Table S4.

The Hf isotopes measured on the 20 dated zircons from the biotite monzogranite sample Y0407 have an upper $^{176}\text{Hf}/^{177}\text{Hf}$ ratio of 0.282496–0.282678 and a lower $^{176}\text{Lu}/^{177}\text{Hf}$ ratio of 0.000865–0.002735. The very low radiogenic Hf concentrations are indicative of zircons crystallising from a magma (Amelin et al., 2000). The $\varepsilon_{\text{Hf}}(t)$ values are positive, ranging from 6.6 to 13, indicating that the monzogranite has a juvenile source. The associated T_{DM1} model age

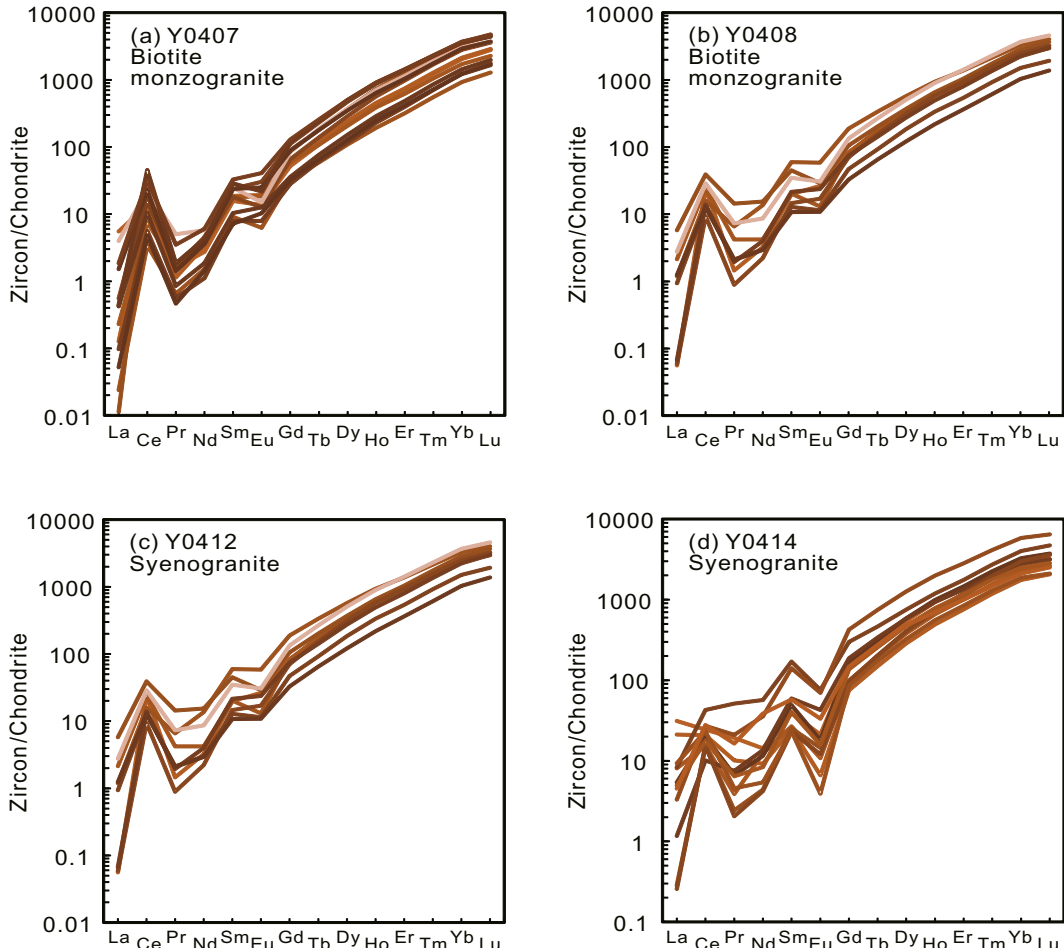


Fig. 6. Chondrite-normalised REE patterns for zircon assays from syenogranite and biotite monzogranite in the Dengganping Complex.

ranges from 1071 to 822 Ma, and the T_{DM2} model age ranges from 1244 to 870 Ma. The Hf isotopes measured on the 20 dated zircons from the biotite monzogranite sample Y0408 have an average high $^{176}\text{Hf}/^{177}\text{Hf}$ ratio of 0.282474–0.282638 and low $^{176}\text{Lu}/^{177}\text{Hf}$ ratio of 0.000842–0.002805. The $\varepsilon_{\text{Hf}}(t)$ values are all positive, ranging from +4.1 to +11.3, indicating it also has a juvenile source. The associated T_{DM1} model age is 1111 to 891 Ma, and the T_{DM2} model age is 1316 to 990 Ma.

The Hf isotopes measured on the 20 dated zircons from syenogranite sample Y0412 have an average high $^{176}\text{Hf}/^{177}\text{Hf}$ ratio of 0.282319–0.282457 and low $^{176}\text{Lu}/^{177}\text{Hf}$ ratio of 0.001165–0.003327. The $\varepsilon_{\text{Hf}}(t)$ values range from -1.7 to 5.1, the associated T_{DM1} model age is 1396 to 1185 Ma, and the T_{DM2} model age is 1735 to 1382 Ma. Zircons from syenogranite sample Y0414 have a high $^{176}\text{Hf}/^{177}\text{Hf}$ ratio of 0.282274–0.282433 and low $^{176}\text{Lu}/^{177}\text{Hf}$ ratio of 0.001028–0.003299. The $\varepsilon_{\text{Hf}}(t)$ values range from -1 to 5.2, which are characteristic of a juvenile source. The associated T_{DM1} model age varies from 1440 to 1179 Ma, and the T_{DM2} model age varies from 1767 to 1382 Ma.

4.4. Zircon O isotopes

Eighty in-situ O isotope analyses of zircons were completed on 80 SIMS U—Pb dates. Except for four O isotope analyses that have high 2σ values, the remaining data are adopted in the following discussion. The zircon O isotope analyses are presented in Table S5.

Zircon ^{18}O values from the biotite monzogranite sample Y0407 limited between 5.13 and 6.75‰. Zircon from the biotite monzogranite sample Y0408 have ^{18}O values between 3.44 and 6.67‰ with five low- ^{18}O zircon grains. Syenogranite samples Y0412 and Y0414 have ^{18}O values between 5.13 and 7.38‰ (Table S5).

4.5. Whole-rock geochemistry

4.5.1. Major elements

The major element assays for the granites are presented in Table S5. The biotite monzogranite has higher SiO_2 assays of 66.7–72.4%, $\text{Na}_2\text{O} + \text{K}_2\text{O}$ values of 6.9–7.8% and Al_2O_3 assays of 14.4–17.2%, and low assays of CaO (1.3–3.1%), MgO (0.7–1.1%), FeO_{T} (2.2–3.4%) and P_2O_5 (0.07–0.11%). The biotite monzogranite has an A/NK value between 1.9 and 2.4, aluminium saturation index (ASI = molar $\text{Al}_2\text{O}_3/(\text{CaO} + \text{Na}_2\text{O} + \text{K}_2\text{O})$) value of 1.6–1.7, and a Rittmann Index ($\sigma = (\text{Na}_2\text{O}$ wt% + K_2O wt%) $^2/(\text{SiO}_2$ wt%–43)) of 1.8–2. The sample plots in the granite field on the SiO_2 vs $(\text{Na}_2\text{O} + \text{K}_2\text{O})$ diagram in Fig. 7(a), calc-alkaline and high-K calc-alkaline fields on the K_2O vs SiO_2 diagram in Fig. 7(b, c), and peraluminous field on the A/NK vs A/CNK diagram in Fig. 7(d). These chemical parameters indicate that the biotite monzogranite is peraluminous and calc-alkaline to high-K calc-alkaline. The biotite monzogranite's estimated temperature of crystallisation, based on the Zr saturation temperature thermometry, is between 731 and 756 °C.

The syenogranite has an A/NK value of 1.6, ASI values of 1.5–1.6%, and a Rittmann Index of 1.9–2.3. The syenogranite plots in the granite field on the SiO_2 vs $(\text{Na}_2\text{O} + \text{K}_2\text{O})$ diagram in Fig. 7(a), the high-K calc-alkaline fields on the K_2O vs SiO_2 diagram in Fig. 7(c), and the peraluminous field on the A/NK vs A/CNK diagram in Fig. 7(d). The syenogranite's estimated temperature of crystallisation, based on the Zr thermometry, is 815–850 °C.

The samples from the Dengganping Complex have similar major element assays (Fig. 8). Coincidentally, granites in the Pengguan Complex to the north and the Kangding Complex to the SW are also peraluminous (Chen et al., 2004; Zhao et al., 2006).

4.5.2. REEs and trace elements

Trace element assays for the granitic samples from the Dengganping Complex are presented in Table S7 and the Chondrite normalised values are plotted in Fig. 8. The total REE content of the biotite monzogranite is between 69.4 and 97.6 ppm and has higher LREE/HREE ratios of 9.9–14.6 and $(\text{La/Yb})_{\text{N}}$ values of 10.5–17.2, enriched LREEs, depleted

HREEs, and weakly depleted δEu and δCe values (Fig. 8a). The plots in Fig. 8(c) show that the biotite monzogranite is relatively enriched in Rb, Ba, Th, U, and K, and depleted in Nb, Ta, P and Ti. The large ion lithophile elements (LILE) are steep and the high field strength elements (HFSE) form a flattened pattern in Fig. 8.

The syenogranite from the Dengganping Complex is significantly different from the biotite monzogranite having a high total REE content of 86.6–151.9 ppm, LREE enrichment, and HREE depletion. The $(\text{La/Yb})_{\text{N}}$ value is 5.4–9.1 coinciding with the flat HREE plot in Fig. 8(a), and an Eu negative anomaly with a δEu value of 0.4–0.5. Fig. 8(c) also shows that the syenogranite is strongly depleted in P and Ti, weakly depleted in Nb and Ta, and enriched in Th, U, Zr, Hf, Sm, Eu, Y, Yb and Lu compared to the biotite monzogranite. On a more regional scale (Fig. 8b, d), the normalised REE patterns of the biotite monzogranite are like those of the monzogranite in the Pengguan Complex to the northwest. The δEu values, and the trace element geochemistry of the biotite monzogranite are also similar to those of the monzogranite in the Pengguan Complex (Fig. 8e, f).

4.6. Whole-rock Nd isotopes

The initial Nd isotopes were recalculated at 742 and 743 Ma for the biotite monzogranite samples, and 815 and 805 Ma for the syenogranite samples. Two of the samples from the biotite monzogranites have relatively homogeneous initial $^{143}\text{Nd}/^{144}\text{Nd}$ ratios of 0.512178–0.512181 and $\varepsilon_{\text{Nd}}(t)$ values that range from -0.7 to +0.5 (Table S8). The syenogranite samples have low and constant initial $^{143}\text{Nd}/^{144}\text{Nd}$ ratios of 0.512056–0.512093 and uniform negative $\varepsilon_{\text{Nd}}(t)$ values of -3.4 to -1.8.

5. Discussion

5.1. Emplacement ages

The western margin of the Yangtze Block is characterised by numerous felsic intrusions associated with many mafic to ultramafic plutons and sparse outcrops of Neoproterozoic volcano-sedimentary units (Li et al., 2008 and references therein). The published dates for the igneous rocks in the region are included in Table 2, their locations are shown in Fig. 9, and their age spread is summarised in Fig. 10.

The nature of the concentrically zoned of the zircons in CL images and Th/U ratios determined by this study are interpreted as being indicative of a magmatic origin (Fig. 4, Tables 1 and 2). The SIMS and LA-ICP-MS zircon U—Pb ages from two biotite monzogranite samples (Y0407, Y0408) yield concordant dates of 747 ± 6 , 743 ± 4 , 742 ± 25 , and 742 ± 5 Ma (Fig. 5). The SIMS and LA-ICP-MS zircon U—Pb dates from two syenogranite samples (Y0412, Y0414) have concordant ages of 811 ± 7 , 815 ± 4 , 806 ± 6 , and 805 ± 4 Ma. All of these dates indicated that the granites in the Dengganping Complex record magmatic events dated at ca. 815 and 740 Ma. Therefore, the complex provides a very good window and probe into the Neoproterozoic evolution of the western margin of Yangtze Block.

Various ca. 825 and 710 Ma igneous rocks are present along the western margin of the Yangtze Block (Figs. 9 and 10). Examples are the 803 ± 12 Ma bimodal volcanic successions in the Suxiong Formation, 799 ± 8 Ma basalt in the Huangshuihe Group, ca. 796 Ma basalt in the Kangding Complex, 808 ± 12 Ma gabbro at Lengqi, 801 ± 7 Ma A-type granite at Xiatianba, 803 ± 15 Ma granite at Xiacun, 806 ± 4 Ma gabbro at Lengshuiqing, 752 ± 11 Ma gabbro at Shaba, and 746 ± 10 Ma gabbro at Dadukou (Guo et al., 2007; Li et al., 2003a, 2003b, 2003c; Ren et al., 2013; Wu et al., 2014; Zhou et al., 2002; Zhou et al., 2006). In addition, extensive middle Neoproterozoic magmatic bodies are broadly coeval with the Dengganping Complex in the western part of the Yangtze Block (Fig. 9), and the spread of these dates is summarised by Fig. 10. These figures show that there was continuous

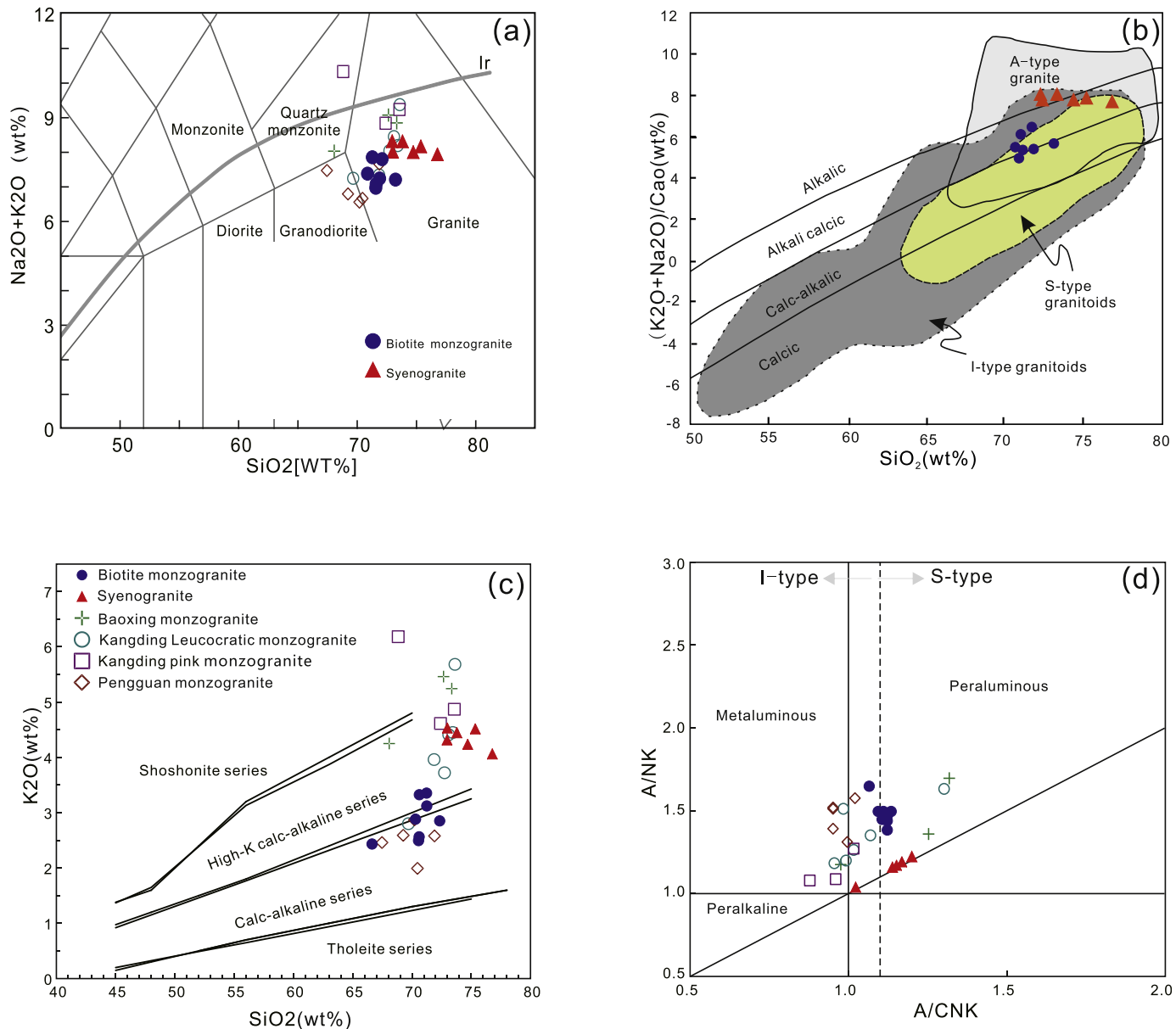


Fig. 7. Diagrams: (a) $(\text{Na}_2\text{O} + \text{K}_2\text{O})$ vs SiO_2 diagram (after Middlemost, 1994); (b) $\text{K}_2\text{O} + \text{Na}_2\text{O}/\text{CaO}$ vs SiO_2 (after Peccerillo and Taylor, 1976); (c) K_2O vs SiO_2 ; and (d) A/NK vs A/CNK (after Maniar and Piccoli, 1989; Peccerillo and Taylor, 1976; Middlemost, 1985).

magmatic activity around the margin of the Yangtze Block between ca. 825 and 710 Ma.

5.2. Petrogenesis

Breiter et al. (2014) proposed that the Zr/Hf ratio of zircons can be divided into common granites ($\text{Zr}/\text{Hf} > 55$), moderately evolved granites ($25 < \text{Zr}/\text{Hf} < 55$) and highly evolved granites ($\text{Zr}/\text{Hf} < 25$). The syenogranite and biotite monzogranite in the Dengganping Complex plot into the moderately evolved granite field, which is important for the reasons outlined below (Fig. 11).

The geochemical classification of igneous rocks of unknown tectonic affinity solely based on discrimination diagrams are inherently inaccurate and open to criticism, because they commonly only use two or three elements, are not statistically rigorous, are based on non-altered rocks, or are formulated using data from restricted areas. After the initial classification of I- and S-type granites by Chappell and White (1974), and additions by various authors that followed them, it is now evident

that the ‘classical’ I-, S-, M-, A-type granitic classifications do not take into account processes such as fractional crystallisation, metamorphism and deformation that might make their application questionable (Barbarin, 1999; Frost et al., 2001; Loiselle and Wones, 1979; White, 1979). For example, highly fractionated “I-type” granites are commonly interpreted as “S-type” or “A-type” granites purely on their geochemistry (Fig. 11a; Chappell, 1999; Wu et al., 2007a; Gao et al., 2016). It should be noted here that discrimination diagrams based on geochemistry have been applied in studies of granites worldwide since the 1970s. The generally accepted premise has been that the composition of a granite reflects its original source (Chappell and White, 1974).

Since the classification of Chappell and White (1974), peraluminous granites with A/CNK values of >1.1 are commonly interpreted as “S-type” granites and A/CNK values of <1.1 are “I-type” granites. However, peraluminous granites may represent fractional crystallisation of metaluminous magma, removal of volatile alkalis complexes phases from Al-saturated magmas, melting of pelitic rocks, or contamination by pelitic country rocks (e.g. Cawthorn et al., 1976; White and

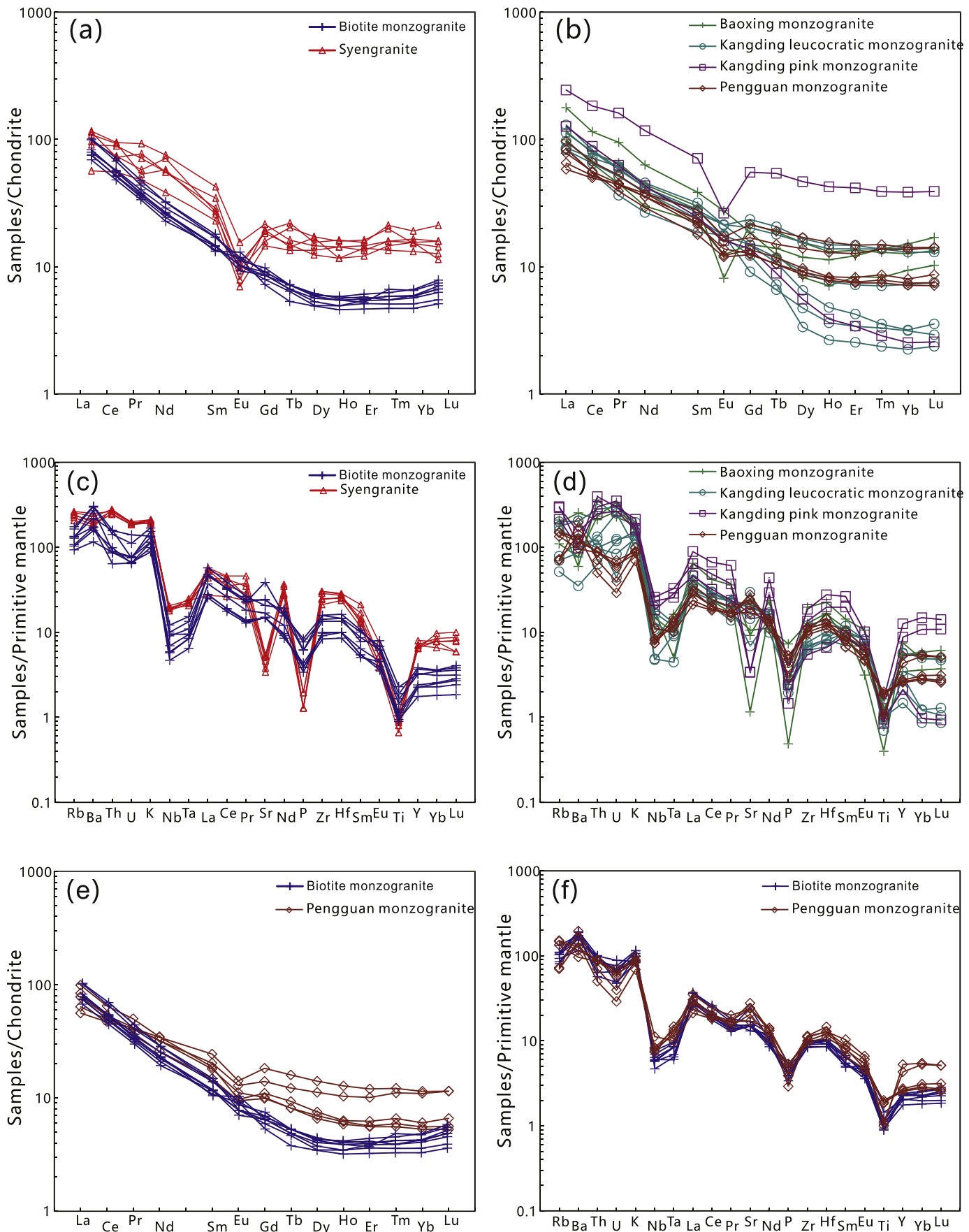


Fig. 8. Chondrite-normalised REE patterns and Primitive mantle-normalised trace element spider diagrams for granitic plutons in the Dengganping Complex and other granitic rocks in the study area. Normalised values are from Sun and [Sun and McDonough \(1989\)](#).

Table 2

Neoproterozoic igneous rocks along the western and northern margins of the Yangtze Block.

Unit	Rock type	Age (Ma)	Error (Ma)	Method	Reference
Duchongshan intrusion	Ultramafic rock	632	6	SIMS	Wang et al. (2013)
Wangmuguan intrusion	Gabbro	635	5	SHRIMP	Liu et al. (2006)
Yaolinghe Group	Rhyolitic tuff	635	6	SIMS	Liu and Zhang (2013)
Zhou'an intrusion	Granite	637	4	LA-ICP-MS	Wang et al. (2013)
Wudang intrusion	Mafic dyke	650	7	SIMS	Li and Zhao (2016)
Yaolinghe Group	Rhyolite	682	6	LA-ICP-MS	Ling et al. (2007)
Fengzishan intrusion	Granodiorite	683	4	LA-ICP-MS	Li (2003)
Yaolinghe Group	Rhyolite	686	3	LA-ICP-MS	Ling et al. (2007)
Gangou intrusion	Granodiorite	701	8	LA-ICP-MS	Li (2003)
Ankang intrusion	Diorite	702	4	LA-ICP-MS	Yang et al. (2012b)
Tiewadian Complex	Granite	704	4	LA-ICP-MS	Yang et al. (2012b)
Gangou intrusion	Quartz diorite	705	4	LA-ICP-MS	Hu (2013)
Wudang intrusion	Granodiorite	705	0.5	LA-ICP-MS	Wang et al. (2017a, 2017b)
Xishenba intrusion	Monzogranite	706	9	LA-ICP-MS	Dong et al. (2012)
Wudang intrusion	Orthogneiss	707	0.1	LA-ICP-MS	Wang et al. (2017a, 2017b)
Xixiang intrusion	Syenogranite	707	20	LA-ICP-MS	Dong et al. (2012)
Sangouping intrusion	Diorite	708	7	LA-ICP-MS	Li (2003)
Wudang intrusion	Orthogneiss	711	2	LA-ICP-MS	Wang et al. (2017a, 2017b)
Xixia intrusion	Granite	714	7	LA-ICP-MS	Li et al. (2010)
Yaolinghe intrusion	Orthogneiss	714	7	SIMS	Liu and Zhang (2013)
Wudang intrusion	Orthogneiss	715	1	LA-ICP-MS	Wang et al. (2017a, 2017b)
Wudang intrusion	Orthogneiss	716	1	LA-ICP-MS	Wang et al. (2017a, 2017b)
Yaolinghe intrusion	Orthogneiss	718	16	SIMS	Liu and Zhang (2013)
Yaolinghe intrusion	Meta-granodiorite	718	33	SIMS	Liu and Zhang (2013)
Yaolinghe Group	Meta-rhyolitic tuff	719	6	SIMS	Liu and Zhang (2013)
Mianning intrusion	Orthogneiss	721	52	SHRIMP	Chen et al. (2004)
Tiewadian Complex	Granite	721	5	LA-ICP-MS	Yang et al. (2012b)
Xixia intrusion	Granite	721	9	LA-ICP-MS	Li et al. (2003c)
Yaolinghe intrusion	Meta-granite	721	9	SIMS	Liu and Zhang (2013)
Ankang intrusion	Diorite	722	8	LA-ICP-MS	Yang et al. (2012b)
Tiewadian Complex	Granite	722	8	LA-ICP-MS	Yang et al. (2012b)
Yaolinghe Group	Meta-rhyolitic tuff	723	18	SIMS	Liu and Zhang (2013)
Hannan intrusive	Gabbro amphibolite	726	38	LA-ICP-MS	Dong et al., 2012
Wudang Group	Meta-lava	726	17	LA-ICP-MS	Zhu et al. (2008)
Wudang Group	Metavolcanic	726	10	LA-ICP-MS	Wang et al. (2013)
Yaolinghe Group	Meta-rhyolitic tuff	726	5	SIMS	Liu and Zhang (2013)
Suixian Group	Tuffaceous siltstone	727	5	SIMS	Yang et al. (2016)
Erliba intrusive	Adakite	730	6	LA-ICP-MS	Liu and Zhao (2013)
Yaolinghe Group	Felsic volcanic rock	731	11	LA-ICP-MS	Zhu et al. (2014)
Gangou intrusion	Quartz diorite	735	3	LA-ICP-MS	Hu (2013)
Sangouping intrusion	Quartz diorite	735	4	LA-ICP-MS	Hu (2013)
Wudumen intrusion	Granite	735	8	LA-ICP-MS	Liu and Zhao et al. (2013)
Yaolinghe Group	Felsic volcanic rock	735	10	SIMS	Zhu et al. (2014)
Yaolinghe Group	Felsic volcanic rock	737	11	LA-ICP-MS	Zhu et al. (2014)
Dadukou intrusion	Gabbro	738	23	SHRIMP	Zhao and Zhou (2007)
Panzhihua intrusion	Olivine gabbro	738	23	SHRIMP	Zhao and Zhou (2007)
Mihunzhen intrusion	Quartz diorite	740	4	LA-ICP-MS	Yan et al. (2014)
Suixian Group	Andesite	741	7	SHRIMP	Xue et al. (2011)
Ankang intrusion	Quartz monzonite	742	5	LA-ICP-MS	Yang et al. (2012a)
Lengshuigou intrusion	Monzogranite	742	2	LA-ICP-MS	Hu et al. (2016)
Suixian Group	Rhyolite	742	6	SIMS	Yang et al. (2016)
Tiewadian Complex	Granite	742	5	LA-ICP-MS	Yang et al. (2012b)
Dadukou intrusion	Gabbro	746	10	SHRIMP	Zhao and Zhou (2007)
Luojiaba intrusion	Gabbro	746	4	SHRIMP	Zhao and Zhou (2009)
Panzhihua intrusion	Hornblende gabbro	746	10	SHRIMP	Zhao and Zhou (2007)
Wudang Group	Keratophyre	747	5	LA-ICP-MS	Zhu et al. (2008)
Yaolinghe Group	Meta-rhyolitic tuff	747	5	SIMS	Liu and Zhang (2013)
Luding intrusion	Granodiorite	748	11	LA-ICP-MS	Lai et al. (2015)
Wenchuan intrusion	Granite	748	7	SHRIMP	Zhou et al. (2006)
Xuelongbao intrusion	Adakite	748	7	SHRIMP	Zhou et al. (2006)
Wudang Group	Tuff	749	8	LA-ICP-MS	Ling et al. (2007)
Kangding intrusion	Granite	751	10	SHRIMP	Li et al. (2003c)
Shaba intrusion	Gabbro	752	12	SHRIMP	Li et al. (2003c)
Shaba intrusion	Gabbro	752	11	SHRIMP	Li et al. (2003c)
Wudang Group	Rhyolite	752	3	LA-ICP-MS	Ling et al. (2007)
Youshui intrusion	Gabbro	752	6	LA-ICP-MS	Dong et al. (2011)
Lengshuigou intrusion	Gabbro	753	4	LA-ICP-MS	Dong et al. (2017)
Zhongziyuan intrusion	Gabbro	753	4	LA-ICP-MS	Gan et al. (2017)
Luding intrusion	Monzodiorite	754	10	LA-ICP-MS	Lai et al. (2015)
Kangding intrusion	Granodiorite	755	6	SHRIMP	Li et al. (2003c)
Sangouping intrusion	Diorite	756	19	LA-ICP-MS	Li et al. (2003c)
Wudang Group	Rhyolite	757	5	LA-ICP-MS	Ling et al. (2007)
Wudang Group	Tuff	757	2	LA-ICP-MS	Ling et al. (2007)
Yaolinghe Group	Meta-rhyolitic tuff	757	9	SIMS	Liu and Zhang (2013)

(continued on next page)

Table 2 (continued)

Unit	Rock type	Age (Ma)	Error (Ma)	Method	Reference
Datian intrusions	Adakite	759	11	SHRIMP	Li et al. (2003c)
Datian dyke	Dolerite	760	4	SIMS	Yang et al. (2017)
Datian intrusion	Adakite	760	4	SHRIMP	Zhao and Zhou (2007)
Sunjiahe Formation	Tuff	760	5	LA-ICP-MS	Deng et al. (2013)
Tongde dyke	Dolerite	760	5	SIMS	Yang et al. (2017)
Wudang Group	Keratophyre	760	9	LA-ICP-MS	Zhu et al. (2008)
Xixiang volcanic	Tuff	760	5	LA-ICP-MS	Deng et al. (2013)
Yaolinghe Group	Meta-rhyolitic tuff	760	5	SIMS	Liu and Zhang (2013)
Dengxiangying intrusion	Gabbro	761	14	SHRIMP	Zhu et al. (2008)
Tianpinghe intrusion	Granite	762	4	SHRIMP	Zhao and Zhou (2009)
Suixian Group	Rhyolite	763	7	SHRIMP	Xue et al. (2011)
Miyi intrusion	Orthogneiss	764	9	SHRIMP	Zhou et al. (2002)
Mujiaba intrusion	Gabbro	764	4	LA-ICP-MS	Dong et al. (2012)
Xixiang intrusion	Diorite	764	9	SHRIMP	Zhao et al. (2010)
Kangding intrusion	Gneissic granite	765	6	SHRIMP	Zhao et al. (2006)
Tiefodian intrusion	Gneissic quartz diorite	765	6	LA-ICP-MS	Hu et al. (2016)
Hannan intrusion	Monzogranite	766	24	LA-ICP-MS	Dong et al. (2012)
Mianning intrusion	Granite	767	20	LA-ICP-MS	Huang et al. (2008)
Kangding intrusion	Diorite	768	7	SHRIMP	Li et al. (2003c)
Yaolinghe Group	Felsic volcanic rock	768	7	LA-ICP-MS	Zhu et al. (2014)
Baoxing intrusion	Granite	769	5	LA-ICP-MS	Meng et al. (2015)
Wudang Group	Tuff	769	33	LA-ICP-MS	Ling et al. (2007)
Taojiaba intrusion	Granodiorite	770	3	LA-ICP-MS	Luo et al. (2018)
Lianhuashan intrusion	Granite	771	17	LA-ICP-MS	Liu et al. (2017)
Baoxing intrusion	Granite	773	5	LA-ICP-MS	Meng et al. (2015)
Mianning intrusion	Granite	773	31	SHRIMP	Huang et al. (2008)
Dengxiangying intrusion	Mafic dyke	774	10	SHRIMP	Ren et al. (2013)
Huangguan intrusion	Syenogranite	774	4	LA-ICP-MS	Luo et al. (2018)
Xiajiang intrusion	Granite	774	7	LA-ICP-MS	Wang et al. (2010)
Xide intrusion	Mafic dyke	774	10	SHRIMP	Ren et al. (2013)
Miyi intrusion	Diorite	775	8	SHRIMP	Li et al. (2003c)
Qixitian intrusion	Granite	775	7	LA-ICP-MS	Zheng et al. (2008)
Bikou volcanic	Tuff	776	13	SHRIMP	Yan et al. (2004)
Huangguan intrusion	Monzogranite	777	8	LA-ICP-MS	Dong et al. (2012)
Lianhuashan intrusion	Granite	777	7	LA-ICP-MS	Xue et al. (2010)
Wudang Group	Metavolcanic	777	6	LA-ICP-MS	Zhu et al. (2008)
Panzhihua intrusion	Trondhjemite	778	11	SHRIMP	Geng et al. (2006)
Jinhekou volcanic	Tuff	779	16	SHRIMP	Xiong et al. (2013)
Luding intrusion	Granite	779	6	SHRIMP	Lin et al. (2006)
Ganluo volcanic	Tuff	780	3	LA-ICP-MS	Jiang et al. (2016)
Kangding volcanic	Dacite	780	12	SHRIMP	Zhuo et al. (2017)
Kangding intrusion	Mafic dyke	780	20	SHRIMP	Lin et al. (2007)
Mianning intrusion	Granite	780	22	SHRIMP	Huang et al. (2008)
Chengjiang volcanic	Tuff	781	11	SHRIMP	Cui et al. (2013)
Bijigou intrusion	Gabbro	782	10	SHRIMP	Zhou et al. (2002)
Mopanshan intrusion	Adakite	782	6	SHRIMP	Huang et al. (2009)
Tiechuanshan intrusion	Granite	782	4	LA-ICP-MS	Luo et al. (2018)
Yanbian volcanic	Basalt	782	53	SHRIMP	Du et al. (2006)
Wangjiangshan intrusion	Gabbro	784	6	LA-ICP-MS	Dong et al. (2011)
Yaolinghe Group	Meta-rhyolitic tuff	784	5	SIMS	Liu and Zhang (2013)
Bijigou intrusion	Diorite	785	5	SIMS	Wang et al. (2016)
Qiaojia volcanic	Tuff	785	12	SHRIMP	Lu et al. (2013)
Shimian intrusion	Granite	786	36	SHRIMP	Zhao et al. (2008)
Tiefodian intrusion	Gneissic granodiorite	786	5	LA-ICP-MS	Hu et al. (2016)
Micangshan intrusion	Granodiorite	787	77	LA-ICP-MS	Dong et al. (2012)
Dashigou Formation	Tuff	789	4	LA-ICP-MS	Deng et al. (2013)
Xixiang volcanic	Tuff	789	4	LA-ICP-MS	Deng et al. (2013)
Bikou volcanic	Tuff	790	15	SHRIMP	Yan et al. (2004)
Jiaoziqing volcanic	Basalt	790	20	LA-ICP-MS	Li et al. (2018)
Shimian intrusion	Granite	790	10	SHRIMP	Zhao et al. (2008)
Yaolinghe Group	Meta-rhyolitic tuff	791	11	SIMS	Liu and Zhang (2013)
Dengxiangying dyke	Gabbro	792	13	SHRIMP	Zhu et al. (2008)
Jiaoziqing intrusion	Granite	792	11	LA-ICP-MS	Li et al. (2018)
Shimian intrusion	Gabbro	792	32	SHRIMP	Zhao et al. (2017)
Tangjiagou intrusion	Orthogneiss	794	11	LA-ICP-MS	Zhang et al. (2016)
Tongde dyke	Dolerite	794	6	SIMS	Yang et al. (2017)
Weiyuan intrusion	Granite	794	11	SHRIMP	Gu and Wang (2014)
Jiaoziqing intrusion	Granite	795	6	LA-ICP-MS	Li et al. (2018)
Kangding intrusion	Orthogneiss	795	11	SHRIMP	Zhou et al. (2002)
Youhui intrusion	Dolerite	795	5	LA-ICP-MS	Dong et al. (2011)
Dengxiangying dyke	Dolerite	796	6	LA-ICP-MS	Cui et al. (2015)
Kangding intrusion	Orthogneiss	796	13	SHRIMP	Zhou et al. (2002)
Shimian intrusion	Gabbro	796	15	SHRIMP	Zhao et al. (2017)
Tongde intrusion	Picrite	796	5	SIMS	Li et al. (2010)
Xide intrusion	Mafic dyke	796	6	LA-ICP-MS	Cui et al. (2015)
Yanbian dyke	Picrite	796	5	SIMS	Li et al. (2010)

Table 2 (continued)

Unit	Rock type	Age (Ma)	Error (Ma)	Method	Reference
Kangding intrusion	Orthogneiss	797	10	SHRIMP	Zhou et al. (2002)
Songlinping	Felsic tuff	798	8	SHRIMP	Jiang et al. (2012)
Baoxing intrusion	Gabbro	799	5	LA-ICP-MS	Meng et al. (2015)
Baoxing intrusion	Gabbro	799	5	LA-ICP-MS	Meng et al. (2015)
Changshiba volcanic	Meta-basalt	799	8	SHRIMP	Ren et al. (2013)
Xijiaba intrusion	Gabbro	799	5	LA-ICP-MS	Dong et al. (2011)
Kaijianqiao volcanic	Felsic tuff	801	7	SHRIMP	Zhuo et al. (2015)
Xiatianbe intrusion	Granite	801	7	LA-ICP-MS	Wu et al. (2014b)
Ankang intrusion	Diorite	802	16	SHRIMP	Geng (2010)
Baoxing intrusion	Gabbro-diorite	802	6	LA-ICP-MS	Meng et al. (2015)
Baoxing intrusion	Gabbro	802	6	LA-ICP-MS	Meng et al. (2015)
Bikou volcanic	Basalt	802	5	SHRIMP	Lin et al. (2013)
Xiaofeng intrusion	Granite	802	10	SHRIMP	Zhang et al. (2008)
Kangdian volcanic	Rhyolite	803	12	SHRIMP	Li et al. (2005)
Suxiong volcanics	Rhyolite	803	12	SHRIMP	Li et al. (2002b)
Xiacun intrusion	Granite	803	15	SHRIMP	Guo et al. (2007)
Zhonghe volcanic	Felsic tuff	803	9	SHRIMP	Jiang et al. (2012)
Luoci volcanic	Basalt	804	3	LA-ICP-MS	Cui et al. (2015)
Luliang volcanic	Felsic tuff	805	14	SHRIMP	Zhuo et al. (2013)
Kangdian volcanic	Tuff	806	4	LA-ICP-MS	Zhuo et al. (2015)
Gaojiacun intrusion	Diorite	806	4	SHRIMP	Zhou et al. (2006)
Lengshuiqing intrusion	Gabbro	806	4	SHRIMP	Zhou et al. (2006b)
Shimian intrusion	Gabbro	806	11	SHRIMP	Zhao et al. (2017)
Dengxiangying dyke	Dolerite	808	8	LA-ICP-MS	Cui et al. (2015)
Kangding intrusion	Gabbro	808	12	SHRIMP	Li et al. (2002b)
Lengqi intrusion	Gabbro	808	12	SHRIMP	Li et al. (2002b)
Wangjiangshan intrusion	Gabbro	808	14	SHRIMP	Zhou et al. (2002)
Datian dyke	Dolerite	809	8	SIMS	Yang et al. (2017)
Huachanggou dyke	Dolerite	809	15	SHRIMP	Cui et al. (2015)
Shimian dyke	Dolerite	809	8	SHRIMP	Cui et al. (2015)
Bikou volcanic	Rhyolite	811	12	SHRIMP	Wang et al. (2008)
Huachanggou dyke	Dolerite	811	15	SHRIMP	Zhao et al. (2017)
Lengshuiqing intrusion	Diorite	812	3	SHRIMP	Zhou et al. (2006)
Beiba intrusion	Gabbro	814	9	SHRIMP	Zhao and Zhou (2009)
Jiuling intrusion	Granite	815	8	SIMS	Sun et al. (2017)
Sunjiahe Formation	Dacite	815	5	SHRIMP	Cui et al. (2013)
Xixiang volcanic	Dacite	815	5	SHRIMP	Cui et al. (2013)
Daxiangling intrusion	Granite	816	10	SHRIMP	Zhao et al. (2008)
Tiechuanshan Group	Rhyolite	817	5	Single-grain zircon U-Pb	Ling et al. (2003)
Bendong intrusion	Granite	818	10	LA-ICP-MS	Wang et al. (2006)
Eshan intrusion	Granite	819	8	LA-ICP-MS	Hu et al. (2018)
Wangjiangshan intrusion	Diorite	819	10	SHRIMP	Zhou et al. (2002)
Tongde intrusion	Gabbro diorite	820	13	SHRIMP	Sinclair (2001)
Bikou volcanic	Rhyolite	821	7	SHRIMP	Wang et al. (2008)
Bikou volcanic	Rhyolite	821	7	SHRIMP	Wang et al. (2008)
Lengshuiqing intrusion	Gabbro	821	1	Hornblende 40Ar-39Ar	Zhu et al. (2007)
Wangjiangshan intrusion	Gabbro	823	6	SIMS	Wang et al. (2016)
Wangjiangshan intrusion	Diorite	823	6	SIMS	Wang et al. (2016)
Xucun intrusion	Granite	823	8	SHRIMP	Wang et al. (2012)
Xucun intrusion	Granite	823	7	SHRIMP	Wang et al. (2012)
Dengxiangying dyke	Dolerite	824	11	SHRIMP	Cui et al. (2015)
Dengxiangying volcanic	Dacite	824	6	SHRIMP	Ren et al. (2016)
Gongcai intrusion	Orthogneiss	824	14	SHRIMP	Zhou et al. (2002)
Huashan Complex	Basalt	824	9	SHRIMP	Deng et al. (2013)
Xihe intrusion	Gabbro	824	4	LA-ICP-MS	Dong et al. (2012)
Xiuning intrusion	Granite	824	7	LA-ICP-MS	Chen et al. (2008)
Yuanbaoshan intrusion	Ultramafic rock	824	4	SHRIMP	Yao et al. (2014)
Gaojiacun intrusion	Gabbro	825	12	SHRIMP	Zhu et al. (2006)
Tongde intrusion	Diorite	825	7	SHRIMP	Munteanu et al. (2010)
Xiuning intrusion	Granite	825	7	LA-ICP-MS	Chen et al. (2008)
Yiyang intrusion	Ultramafic rock	826	3	SHRIMP	Liu et al. (2006)
Guibei intrusion	Granite	827	7	SIMS	Zhao et al. (2013)
Sanfang intrusion	Granite	827	15	SHRIMP	Li (1999)
Xucun intrusion	Granite	827	7	SHRIMP	Wang et al. (2012)
Yaojinghe intrusion	Diorite	827	8	SIMS	Liu and Zhang (2013)
Xihe intrusion	Granite	829	5	LA-ICP-MS	Dong et al. (2012)
Chishuigou intrusion	Gabbro	833	4	LA-ICP-MS	Zhang et al. (2016)
Sunjiahe Formation	Rhyolite	833	5	LA-ICP-MS	Xu et al. (2009)
Xixiang volcanic	Rhyolite	833	5	LA-ICP-MS	Xu et al. (2009)
Yanbian dyke	Diorite	833	15	SHRIMP	Li and Zhao (2018)
Guangwushan intrusion	Syenogranite	838	17	LA-ICP-MS	Dong et al. (2012)
Shatan intrusion	Diorite	840	6	LA-ICP-MS	Dong et al. (2012)
Xixiang volcanic	Basalt	840	10	SHRIMP	Yan et al. (2004)
Mihunzhen intrusion	Diorite	843	5	LA-ICP-MS	Dong and Santosh (2016)
Dadukou volcanic	Basalt	845	17	LA-ICP-MS	Xu et al. (2009)

(continued on next page)

Table 2 (continued)

Unit	Rock type	Age (Ma)	Error (Ma)	Method	Reference
Sunjiahe Formation	Basalt	845	17	LA-ICP-MS	Xu et al. (2009)
Bikou volcanic	Basalt	846	19	SHRIMP	Yan et al. (2004)
Yaolinghe Group	Felsic tuff	847	8	LA-ICP-MS	Zhu et al. (2014)
Baoxing intrusion	Gabbro	848	4	LA-ICP-MS	Meng et al. (2015)
Shenwu volcanic	bimodal volcanic	849	7	SHRIMP	Li et al. (2008)
Guandaoshan intrusion	Diorite	856	6	SHRIMP	Du et al. (2014)
Guandaoshan intrusion	Gabbro	856	8	SHRIMP	Du et al. (2014)
Guandaoshan intrusion	Gabbro	857	13	SHRIMP	Du et al. (2014)
Guandaoshan intrusion	Diorite	857	7	SHRIMP	Du et al. (2014)
Zhengyuan intrusion	Gabbronorite	857	46	LA-ICP-MS	Dong et al. (2012)
Guandaoshan intrusion	Diorite	858	7	SHRIMP	Sun et al. (2008)
Huashan Complex	Granite	858	15	LA-ICP-MS	Xu et al. (2016)
Tiefodian intrusion	Biotite plagiogneiss	858	19	LA-ICP-MS	Zhang et al. (2016)
Datian intrusion	Syenogranite	860	5	LA-ICP-MS	Gan et al. (2016)
Tianpinghe intrusion	Granite	860	6	LA-ICP-MS	Luo et al. (2018)
Huashan Complex	Granite	862	5	LA-ICP-MS	Xu et al. (2016)
Gezong intrusion	Granite	864	8	SHRIMP	Zhou et al. (2002)
Huashan Complex	Granite	866	10	LA-ICP-MS	Xu et al. (2016)
Tiefodian intrusion	Biotite plagiogneiss	868	26	LA-ICP-MS	Zhang et al. (2016)
Beiba intrusion	Diorite	869	5	SIMS	Wang et al. (2016)
Datian intrusion	Syenogranite	869	4	LA-ICP-MS	Gan et al. (2016)
Daheba intrusion	Granodiorite	871	77	LA-ICP-MS	Dong et al. (2012)
Huashan Complex	Gabbro	871	7	LA-ICP-MS	Xu et al. (2016)
Bikou intrusion	Gabbro	877	13	LA-ICP-MS	Xiao et al. (2007)
Beiba intrusion	Gabbro	879	6	LA-ICP-MS	Luo et al. (2018)
Bikou intrusion	Diorite	884	6	LA-ICP-MS	Xiao et al. (2007)
Lengshuigou intrusion	Quartz diorite	884	3	LA-ICP-MS	Hu et al. (2016)
Mihunzhen intrusion	Diorite	885	4	LA-ICP-MS	Yan et al. (2014)
Liushudian intrusion	Gabbro	888	6	SIMS	Zhou et al. (2018)
Micangshan volcanic	Rhyolite	895	3	TIMS	Ling et al. (2003)
Liushudian intrusion	Gabbro	898	10	LA-ICP-MS	Dong et al. (2011)
Yanbian volcanic	Basalt	920	20	SHRIMP	Li et al. (2006)
Chishuigou intrusion	Diorite	925	28	LA-ICP-MS	Zhang et al. (2016)
Lengshuigou intrusion	Diorite	941	3	LA-ICP-MS	Hu et al. (2016)
Micangshan volcanic	Dacite	950	4	TIMS	Ling et al., (2003)

(Chappell, 1977). The implication of this is that the genetic terms “S-” and “I-” types should be used cautiously when talking about granites especially when they are metamorphosed and deformed. Hence, these discrimination diagrams should be used in combination with more robust evidence.

The two granitic suites in the study area are characterised by their different REE signatures, illustrating that they have different magmatic sources. In detail, the ca. 815 Ma syenogranite is significantly different from the ca. 740 Ma biotite monzogranite by plotting in the high-K calc-alkaline field, has an obvious negative Eu anomaly, is strongly depleted in LILEs (Sr, P, and Ti), and enriched in HFSEs (Th, U, Zr, Hf, Sm, Eu, Y, Yb and Lu). The negative Eu anomaly is indicative of plagioclase being separated early from the source magma. Furthermore, the syenogranite has an A-type granite affinity and the biotite monzogranite samples plot in the combined I- and S-type granite fields on the (10,000 Ga/Al) vs Zr, and (Zr + Nb + Ce + Y) vs (K₂O + Na₂O)/CaO) discrimination diagrams in Fig. 11(a–c). This points toward a fractionated magmatic source for the monzogranite (Whalen et al., 1987).

The syenogranite contains enstatite, which is characteristic of A-type granites (Fig. 3b, c; Collins et al., 1982; Whalen et al., 1987). In addition, it can further be subdivided as an A2-type granite on the Y/Nb vs Yb/Ta, Nb-Y-Ce and Nb-Y-3Ga discrimination diagrams (Fig. 11e–f; Eby, 1992).

The I-type classification is applied to granites containing hornblende and biotite, and S-type granites commonly contain combinations of andalusite, cordierite, garnet, and muscovite (Chappell and White, 1992). The biotite monzogranite contains hornblende and biotite and does not contain andalusite, cordierite, garnet, and muscovite, indicating it has an I-type granite affinity (Fig. 3e, f). Yet, the monzogranite's geochemistry indicates it has an S-type affinity contradicting the petrological observations (Fig. 11a, b). Again, this demonstrates the need to be cautious with these classifications (c.f. Whalen et al., 1987). Nonetheless, it

can be said that the monzogranite is a fractionated I-type granite, and the syenogranite has an A-type granite affinity.

5.3. Possible magma source

As discussed above, the biotite monzogranite in the Dengganping Complex is fractionated in LREE and HREE, and has weak δEu and δCe negative anomalies (Fig. 8). In contrast, the syenogranite is different having a higher SiO₂ assay of around 74% (compared to ~70 wt% SiO₂ for the biotite monzogranite), and a higher Y assay. In addition, when comparing the granitic samples from the Dengganping, Baoxing, Kangding and Pengguan complexes on the La vs La/Sm and Zr vs Zr/Sm diagrams in Fig. 11(g, h), the biotite monzogranite from Dengganping has a partially melted source, the Kangding pink monzogranite is fractionally crystallised, and the rest of the samples have a partially melted source, except for the syenogranite from Dengganping that appears to have both a partially melted and fractionally crystallised source. This fractional crystallisation and partial melting of the granites' source must also be considered when using the geochemistry of granites to propose a tectonic setting for the generation of their source (as mentioned above). Granites with an A2-type affinity are derived from melting of continental crust or underplated mafic crust that has been through a cycle of continent-continent collision or island-arc magmatism (Eby, 1992). Following this generalisation, the Dengganping A2-type granites were probably generated by crustal partial melting.

Neodymium and zircon Hf isotopic systematics, and U—Pb dates are commonly used to help determine the source of granitic rocks (e.g. Wu et al., 2003, 2004). The $\varepsilon_{\text{Hf}}(t)$ (−1.7 to +5.2) and negative $\varepsilon_{\text{Nd}}(t)$ (−3.2 to −1.8) values of the Dengganping syenogranite and the relatively high positive $\varepsilon_{\text{Hf}}(t)$ (+6.6 to +13) and $\varepsilon_{\text{Nd}}(t)$ (−0.7 – +0.5) values of the Dengganping biotite monzogranite show that the magma

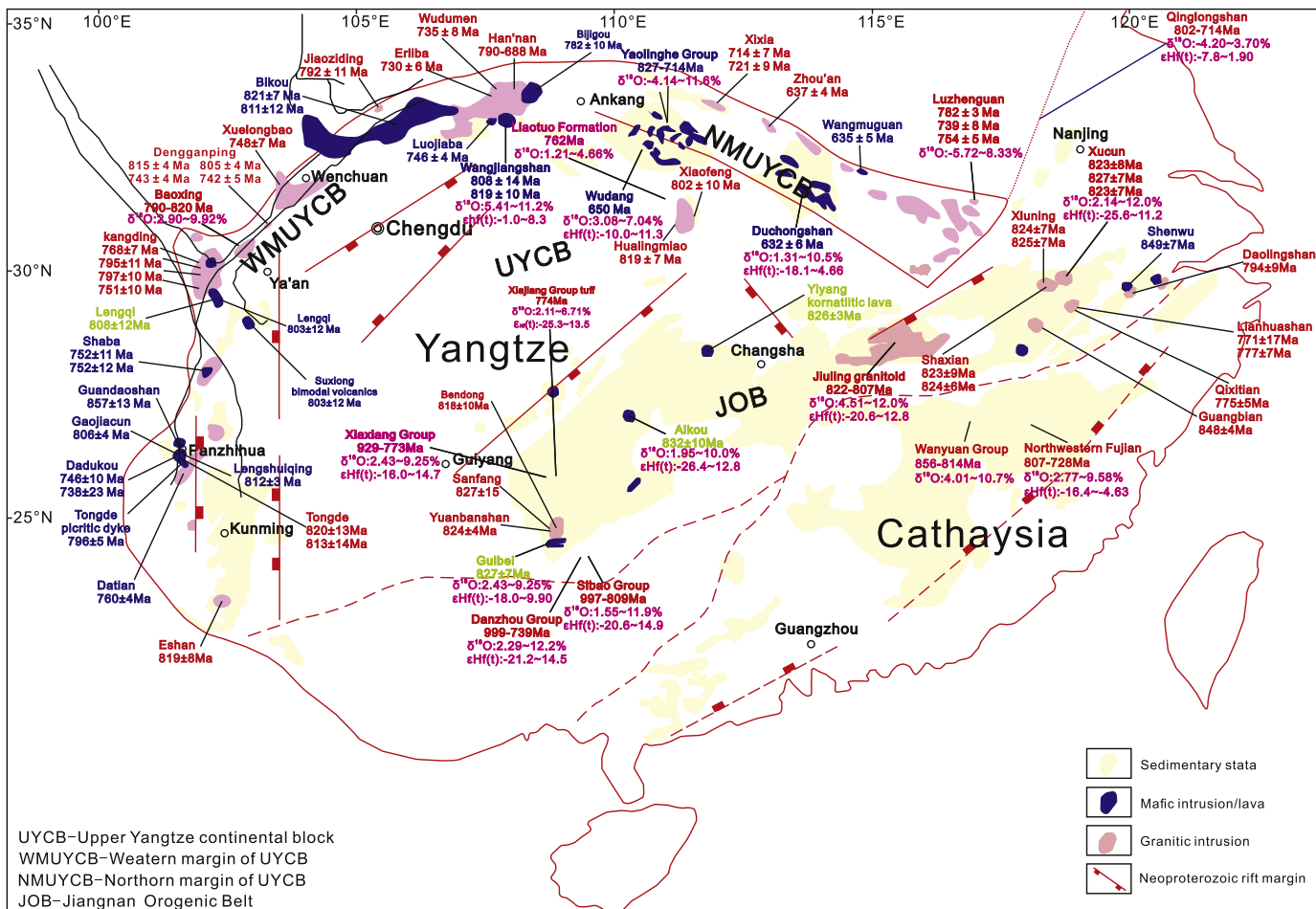


Fig. 9. Distribution of the Neoproterozoic magmatic rocks and their Age-Hf-O results in the Yangtze Block (Data from Huang et al., 2019; Zhao and Guo, 2012; He et al., 2017; Zhou et al., 2006; Zhao et al., 2006; Chen et al., 2004; Pei et al., 2009; Zhou et al., 2002; Dong et al., 2012; Yang et al., 2012b; Wang and Li, 2003; Zhao and Zhou, 2008; Wang et al., 2012; Wang et al., 2013b).

associated with the syenogranite was relatively enriched in Nd—Hf isotopes and the magma represented by the biotite monzogranite was relatively depleted (Fig. 12a, b). This could relate to the relative contributions of crustal and mantle material in the magma sources or during the subsequent emplacement of the granites (Huppert et al., 1985).

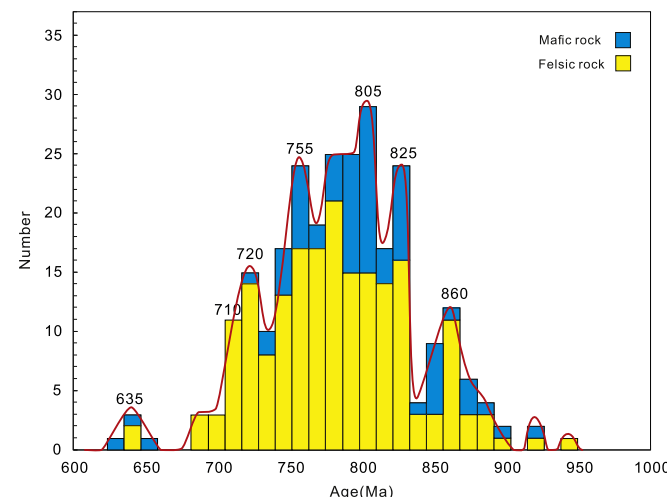


Fig. 10. Cumulative probability diagram of ages of Neoproterozoic magmatic rocks along western and northern margin of Yangtze Block. (references shown in Table 2).

The T_{DM1} model age of the syenogranite ranges from 1440 to 1179 Ma, and the T_{DM2} model age ranges from 1767 to 1382 Ma, indicative of a Paleo- to Mesoproterozoic magmatic source. The biotite monzogranite's T_{DM1} model age ranges from 1315 to 822 Ma, and its T_{DM2} model age ranges from 1411 to 870 Ma. The highest ϵ_{HF} value for the analysed samples is +13, which is very close to the value of +13.8 on the evolution curve of depleted mantle (Fig. 12a; Griffin et al., 2000). We thus propose that the biotite monzogranite was generated by partial melting of a late Mesoproterozoic to early Neoproterozoic mafic crust. Furthermore, the Nd isotope model ages (T_{DM}) of 1780–1560 Ma for the syenogranite and 1420–1270 Ma for the biotite monzogranite are almost the same as those determined from the Hf isotopes (Fig. 12b; Table S8).

5.4. Tectonic implications

Generally speaking, the temperature of the intermediate to felsic magmatic rocks formed by the “mantle plume” is relatively high (>800 °C) (Liu et al., 2013; Wu et al., 2007b). The temperature of a granitic magma formed during the subduction is relatively low in the presence of a large amount of fluid derived from the subducted crust (<800 °C) (Liu et al., 2013; Miller et al., 2003). The estimated crystallisation temperature of the syenogranite and biotite monzogranite, based on the Zr saturation temperature thermometry, ranged from 815 to 850 °C, and 756 to 731 °C, this represents a high temperature thermal event during 815–805 Ma. At least three high-temperature magmatic

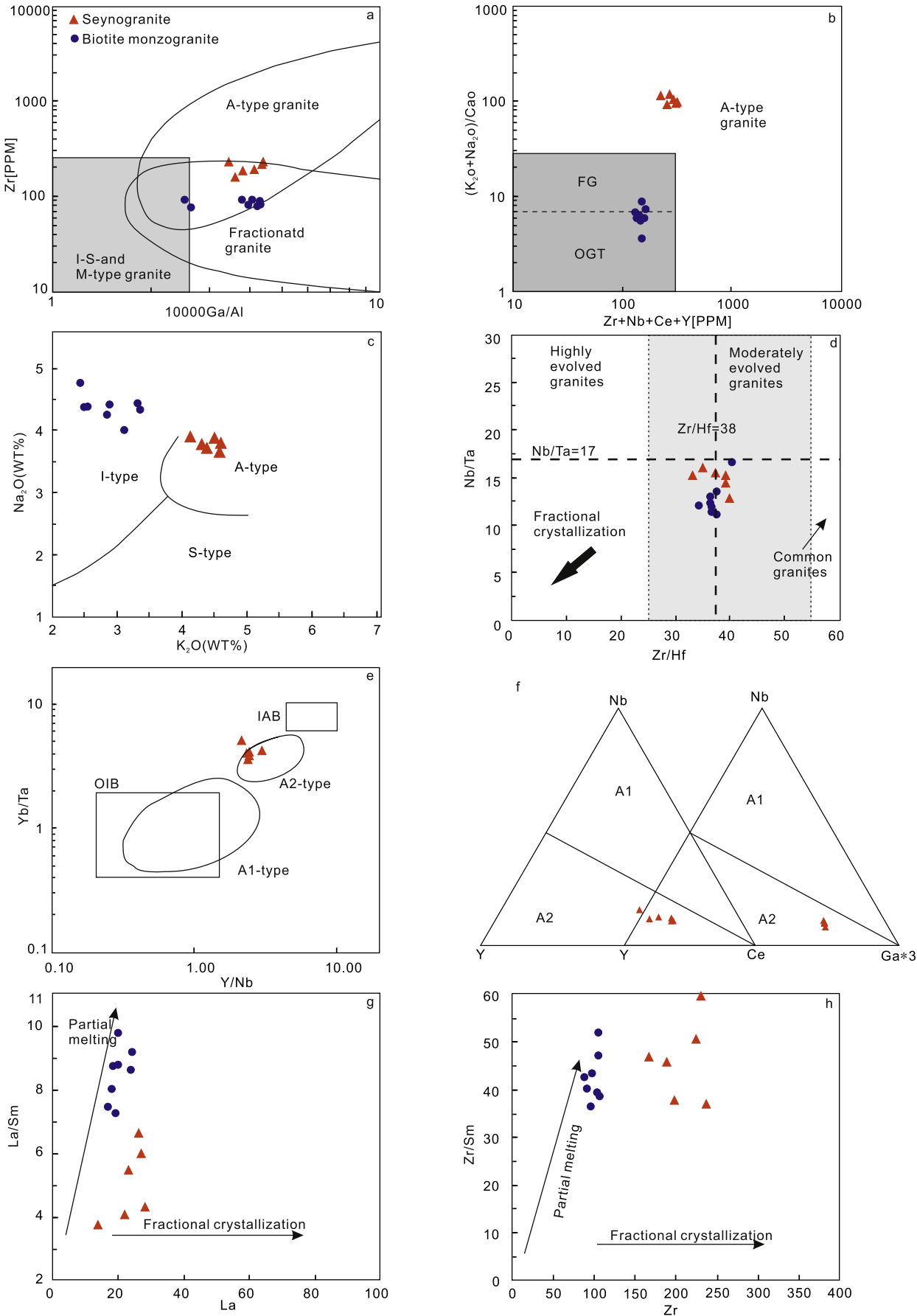


Fig. 11. Diagrams: (a) ($10000\text{Ga}/\text{Al}$) vs Zr (after Whalen et al., 1987); (b) ($Zr + Nb + Ce + Y$) vs $(K_2O + Na_2O)/CaO$ (after Whalen et al., 1987); (c) K_2O/Na_2O (after Collins et al., 1982); (d) Zr/Hf vs Nb/Ta (after Breiter and Škoda, 2017); (e) Y/Nb vs Y/Ta (after Eby, 1992); (f) ($Y + Nb$) vs Rb (after Pearce et al., 1984); (g) La vs La/Sm ; and (h) Zr - Zr/Sm (after Allègre and Minster, 1978).

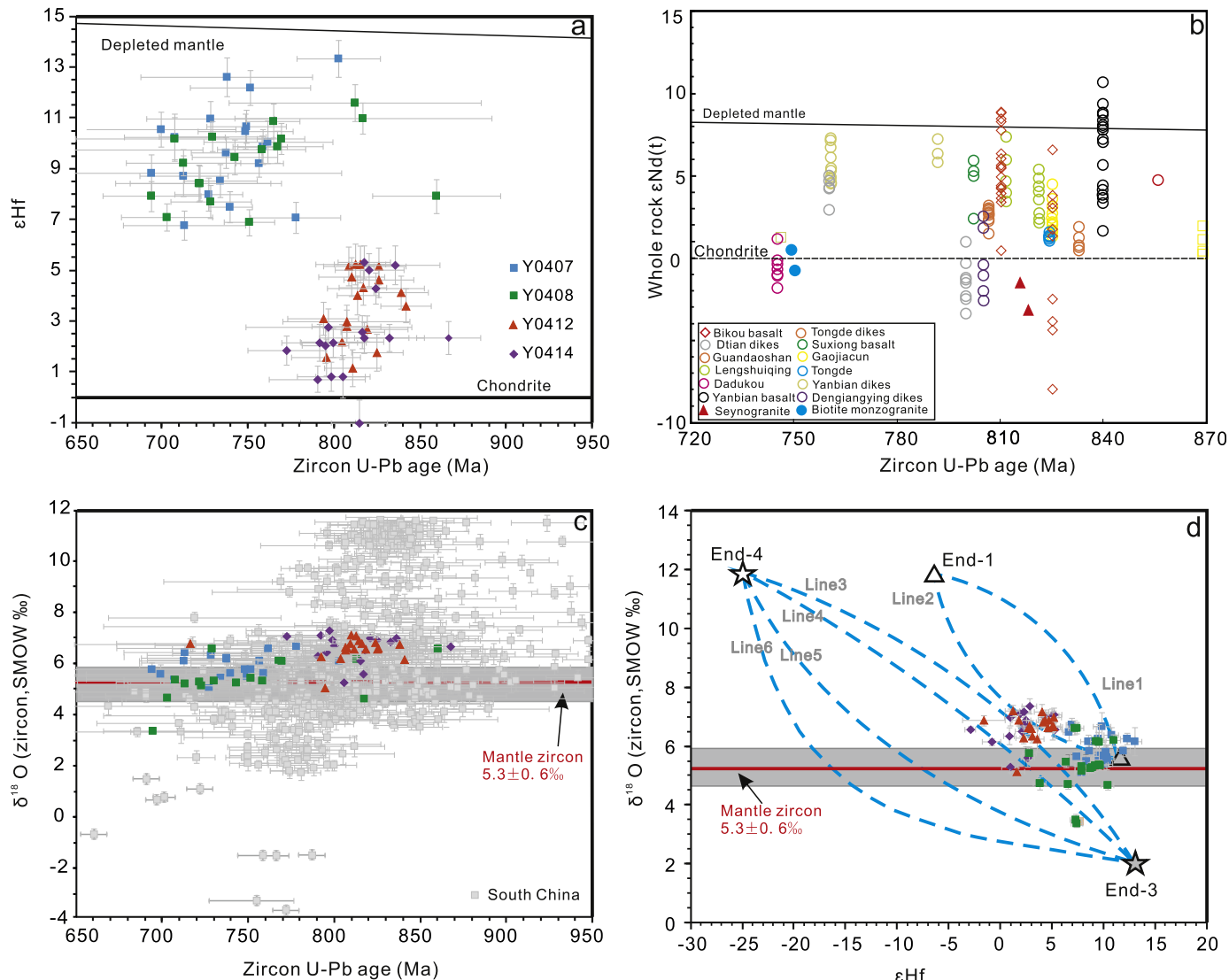


Fig. 12. Diagrams: (a) (Age)- $\varepsilon_{\text{Hf}}(t)$ for Neoproterozoic plutons along the Western margin of Yangtze Block; (b) (Age)- $\varepsilon_{\text{Nd}}(t)$ for Neoproterozoic pluton in the Western margin of Yangtze Block (Data from Zhao et al., 2018); (c) Plots of $\delta^{18}\text{O}$ vs U-Pb dates (Data from Wang et al., 2017a); and (d) Diagrams of $\delta^{18}\text{O}$ vs $\varepsilon_{\text{Hf}}(t)$. End-1 refers to the Neoproterozoic basement sequences with $\varepsilon_{\text{Hf}}(t) = -6.35$ and $\delta^{18}\text{O} = 12\text{‰}$, End-2 refers to Neoproterozoic juvenile crust with $\varepsilon_{\text{Hf}}(t) = 11.6$ and $\delta^{18}\text{O} = 5.6\text{‰}$, End-3 refers to Neoproterozoic altered juvenile crust with $\varepsilon_{\text{Hf}}(t) = 13.3$ and $\delta^{18}\text{O} = 2\text{‰}$, and End-4 refers to Archean basement sequences with $\varepsilon_{\text{Hf}}(t) = -25$ and $\delta^{18}\text{O} = 12\text{‰}$. Line 1 is modelled by End-1 with $\text{Hf}_{\text{pm}}/\text{Hf}_c = 0.28$, and line 2 is modelled by End-2 with $\text{Hf}_{\text{pm}}/\text{Hf}_c = 3.5$. Lines 3, 4, 5, and 6 are modelled by End-3 and End-4 with $\text{Hf}_{\text{pm}}/\text{Hf}_c = 2.14, 0.14, 0.4$, and 1.4 , respectively (after Huang et al., 2019 and Wang et al., 2013). Data from the Kangding Complex are from Huang et al. (2008) and Lin et al. (2007), from the Hannan Complex are from Ao et al. (2014) and Liu et al. (2009a, 2009b), and from the Panzhihua Complex are from Zhao et al., 2008).

events can be distinguished during 897–887, 817–760 and 707–700 Ma based on the whole-rock Zr saturation temperatures of granites analysed from the Yangtze Block (Zhu et al., 2018).

The interpreted tectonic settings for western Yangtze Block, however, are based on the chemistry of multiply deformed and metamorphosed granites that have apparent petrogenesis differing significantly from what is expected for rift-related granites. Neoproterozoic extensional faults of different scales trend east, east-northeast, and northwest in the Yangtze Block, which are delineated from detailed interpretations of deep-seated faults by integrating over 430 sets of 2D seismic data ($>50,000 \text{ km}^2$), 3D seismic data (5000 km^2), and large-scale aeromagnetic data (Gu and Wang, 2014). The emplacement of widespread A-type granitic plutons and bimodal volcanic rocks in the Suxiong Formation along the western margin of Yangtze Block also confirms the presence of Neoproterozoic extensional faults (Li et al., 2002b; Wang et al., 2008). This now poses a significant uncertainty in the current

interpretations of convergent tectonic settings for the western margin of the Yangtze Block during ca. 825–710 Ma.

Magmatic zircon crystallised in magma derived from the crust commonly have $\delta^{18}\text{O}$ values varying from the mantle value of 5.3 ± 0.6 to $14\text{--}16\text{‰}$, with increasing addition of supracrustal material, and magmatic zircons with $\delta^{18}\text{O}$ values lower than the mantle value are rare (Bindeman and Valley, 2002; Huang et al., 2019; Spencer et al., 2017; Valley et al., 1998; Valley et al., 2003; Valley et al., 2005). Magmatic differentiation does not substantially change the oxygen isotope composition of a magma, but high temperature water-rock reactions result in a significant reduction of the oxygen isotope composition of the rocks (Zhang and Zheng, 2011). Low- $\delta^{18}\text{O}$ natural reservoirs are meteoric water with values of -65 to 0‰ and seawater with a value of 0‰ (Bindeman et al., 2008). This means that the formation of low- $\delta^{18}\text{O}$ magmatic rocks requires an oxygen isotope exchange with such a media at elevated temperatures. Hydrothermal alteration with seawater can only result in rocks with low- $\delta^{18}\text{O}$ values, however,

hydrothermal alteration with meteoric water can result in rocks with negative- $\delta^{18}\text{O}$ values (Zheng et al., 2003). In general, an extensional environment, such as a caldera or rift, is proposed as an ideal setting for the coeval development of deep-seated faults and magmatism. This is the most favourable tectonic setting for high-temperature reactions between water and rocks during the genesis of a low- $\delta^{18}\text{O}$ magma (e.g. Bindeman et al., 1998, 2008; Harris and Ashwal, 2002; Tucker et al., 2001; Wang et al., 2011; Watts et al., 2010; Yang et al., 2008; Zhang and Zheng, 2011). Typical examples are the Pleistocene high-temperature rhyolite beds at the Yellowstone National Park, USA, and Paleocene granites in western Scotland, which formed in the extensional setting related to mantle plumes (Bindeman et al., 2008; Monani and Valley, 2001; Watts et al., 2010).

The syenogranite from the Dengganping Complex has zircon ^{18}O values between 5.13 and 7.38‰, and the biotite monzogranite has slightly lower ^{18}O values between 3.44 and 6.67‰ (Fig. 12c). It is acknowledged that the oxygen-isotope systematics of zircons can be affected by the “high-U matrix effect” due to radiation damage (Williams and Herdt, 2000), diffusion rates, degrees of metamictisation and subsequent alteration (Gao et al., 2014). However, The zircons with low $\delta^{18}\text{O}$ values from the biotite monzogranite contain <2000 ppm U, their degree of lattice damage described as “displacements-per-atom (D_{dpa})” is lower than 0.15 (D_{dpa} calculation formula from Gao et al., 2014), and there is no obvious linear relationship between U, D_{dpa} and $\delta^{18}\text{O}$ values of zircons with low $\delta^{18}\text{O}$ values (Fig. 13). Furthermore, the $\delta^{18}\text{O}$ values of the zircons recorded from the biotite monzogranite are lower than the $\delta^{18}\text{O}$ values of the syenogranite zircons.

Zircons with high $\delta^{18}\text{O}$ values are recorded from the syenogranite in the Dengganping Complex indicative of a pre-rift or initial-rift setting with the granite derived from a crustal source, which has experienced a low-T alteration or chemical weathering processes (Zheng et al., 2007). The zircons from the biotite monzogranite have low $\delta^{18}\text{O}$ values and, from our discussion above, is probably derived from an early Neoproterozoic igneous source in the crust (during partial melting resulting from a high-temperature water-rock reaction in an extensional setting). Zircons with low- $\delta^{18}\text{O}$ values are recorded from igneous rocks younger than ca. 800 Ma along the northern margin of the Yangtze and Cathaysia blocks (Huang et al., 2019).

The Hf—O isotopes end-member mixing model by Huang et al. (2019) and Wang et al. (2013) were plotted to explore the origin of the granites with low- $\delta^{18}\text{O}$ values in the Dengganping Complex. The four end-members detected in Fig. 3 are labelled as: End-1 referring to Neoproterozoic metasedimentary country rocks with moderately enriched Hf isotopes and high $\delta^{18}\text{O}$ values; End-2 referring to a Neoproterozoic juvenile crust source with depleted Hf isotopes and mantle-like $\delta^{18}\text{O}$ values; End-3 referring to a Neoproterozoic juvenile crust with depleted Hf isotopes and low $\delta^{18}\text{O}$ values resulting from high-temperature hydrothermal alterations; and End-4 referring to Archean sequences with extremely negative $\varepsilon_{\text{Hf}}(t)$ and high $\delta^{18}\text{O}$ values. The ca. 815 Ma syenogranite follows the lines defined by End-2, indicative of a contribution from a Neoproterozoic juvenile crust.

The ca. 740 Ma biotite monzogranite has a source constrained by End-2 and End-3 (Fig. 12d). The $\delta^{18}\text{O}$ value of End-3 is above zero, suggesting a rifting environment that is favourable for a high-temperature water-rock interaction generating the low-oxygen isotopic values.

Models for the melting of the lower crust are diverse and include delaminating, crustal thickening, and underplating of juvenile basaltic melts at the base of the crust (e.g. Atherton and Petford, 1993; Chung et al., 2003; Li et al., 2003c; Xu, 2002). The delamination model has the lower crust plunging into deep parts of the mantle resulting in partial assimilation with the mantle, and would be characterised by high Mg, Mg#, Cr, Co and Ni values, which is not the case for the granites in the study area. Therefore, the rifting and crustal thickening models are considered here as the most plausible options (c.f. Li et al., 2002a, 2002b, 2003a; Zhu et al., 2004, 2008; Huang et al., 2008).

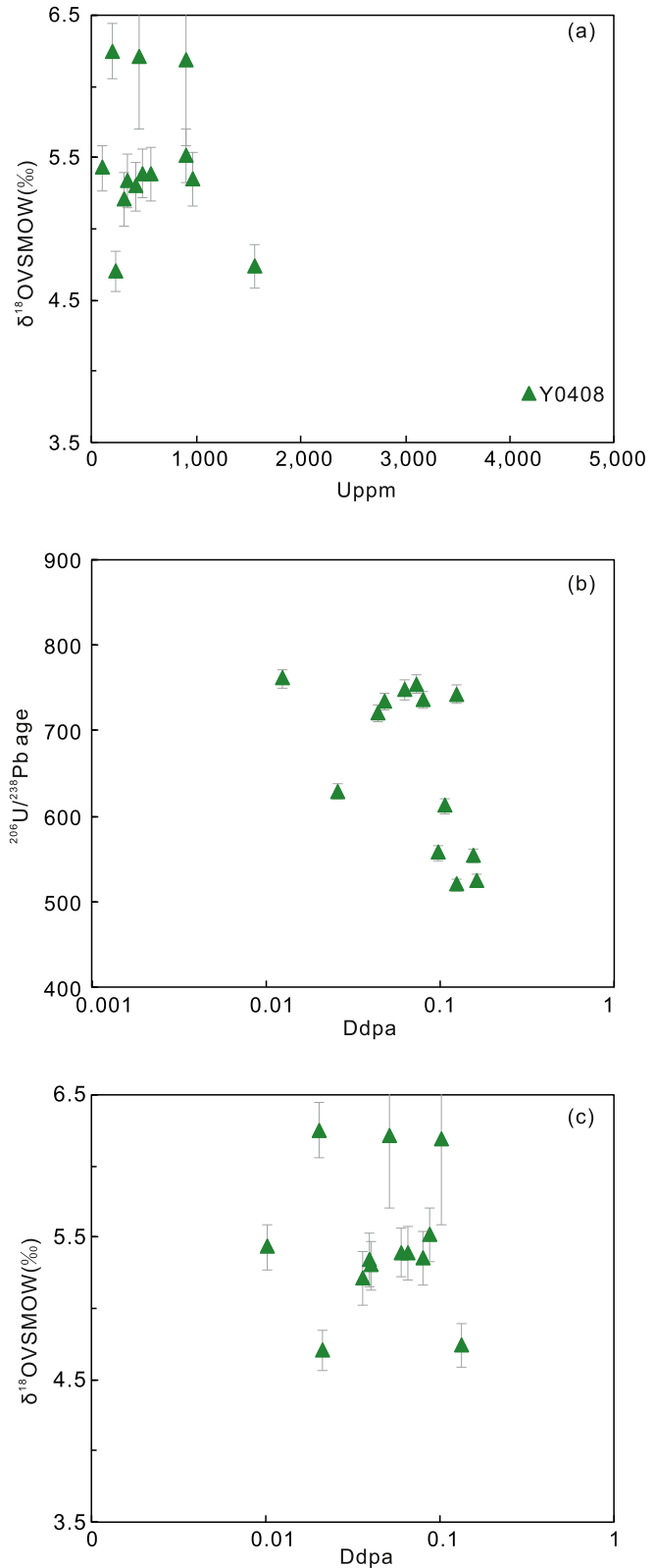


Fig. 13. (a) Plot of zircon U content vs. $\delta^{18}\text{O}$ values; (b) Plot of zircon D_{dpa} vs. $^{206}\text{Pb}/^{238}\text{U}$ age; and (c) Plot of zircon D_{dpa} vs $\delta^{18}\text{O}$ values. The value for D_{dpa} is calculated based on $[U]$, $[Th]$ assays obtained from the corresponding SIMS spots. The calculation formula for D_{dpa} is from Gao et al. (2014).

5.5. Breakup of the Rodinia Supercontinent

Following a period of tectonic stability during the Mesoproterozoic, the Rodinia Supercontinent began to breakup during the Neoproterozoic (Dalziel, 1991; Li et al., 2012; Moores, 1991; Powell et al., 1993; Wan et al., 2019). With the onset of the supercontinent's fragmentation and opening of an unnamed Proto-Tethys Ocean west of South China during ca. 825 Ma (Li, 1999; Li et al., 2003c, 2012; Wan et al., 2019; Zhao et al., 2018), the western margin of the Yangtze Block formed the edge of a continent. It was during this period that the Neoproterozoic granitic and mafic igneous bodies were widely emplaced recording the supercontinent's breakup (Fig. 14). The two widely accepted models posited for the breakup of the Rodinia Supercontinent are:

- (1) Mantle plume developed in the centre of the supercontinent located at the western margin of the Yangtze Block, which was in contact with Australia and North America (e.g. Li, 1999; Li et al., 2003a, 2003b, 2003c; Tian et al., 2017); and
- (2) The western edge of the Yangtze Block was separated from the rest of the supercontinent during extensional tectonics, oceanic subduction and the development of island-arcs and associated granites (e.g. Zhao et al., 2002).

Our geochemical data from the ca. 815 syenogranite and 740 Ma biotite monzogranite can be interpreted as being related to a rift developed in a within-plate tectonic setting rather than the volcanic-arc granites along Longmenshan Fault Zone at the western margin of the Yangtze Block (Lin et al., 2007; Wang et al., 2008; Zhao and Zhou, 2007; Zhou et al., 2006).

Torsvik (2003) used geological and paleomagnetic data to conclude that the Rodinia Supercontinent converged between ca. 1100 and 1000

Ma, and then fragmented during ca. 850–800 Ma. Wang (2000) proposes that the beginning of the supercontinent's fragmentation is approximately 820–800 Ma at around the time the syenogranite was emplaced in the Dengganping Complex. Tian et al. (2017) integrated age data from various regions in China and suggest that the supercontinent broke apart during ca. 820–800 Ma, again broadly coeval with the syenogranite in the Dengganping Complex.

Merdith et al. (2017) also used the ca. 800 Ma date as the starting point for the breakup of the Rodinia Supercontinent when studying the connection between the Australian continent and Laurentia. Mafic dyke swarms dated at ca. 755 Ma in northwestern Australia and ca. 780 Ma in Western North America are coeval with those in the study area and the three mafic events are probably related to mantle plumes (Harlan et al., 2003; Li et al., 2006; Lin et al., 2007; Park et al., 1995). The post-780 Ma tectonostratigraphy of western Laurentia, eastern Australia and South China are widely regarded as correlative (e.g., Li et al., 2008; Wang and Li, 2003). In this model, South China is the “missing link” located between Australia and Laurentia in Rodinia's reconstruction (Li, 1995; Torsvik, 2003).

The proposed tectonic model for the western margin of Yangtze Block is presented in Fig. 14 involving the action of a mantle plume with the opening of the an unnamed Proto-Tethys Ocean and separation of Australia, South China, and Northern America during ca. 825–710 Ma. The establishment of a mantle plume during ca. 825 Ma is expressed by rifting separating Australia from South China and emplacement of bimodal intrusive rocks. Continued rifting powered by the plume resulted in emplacement of gabbroic and syenogranitic magma during ca. 825–805 Ma (Fig. 14a). The last stages of the rifting led to the opening of an unnamed Proto-Tethys Ocean and during ca. 750–710 Ma accompanied by the emplacement of the biotite monzogranite in the Dengganping Complex (Fig. 14b).

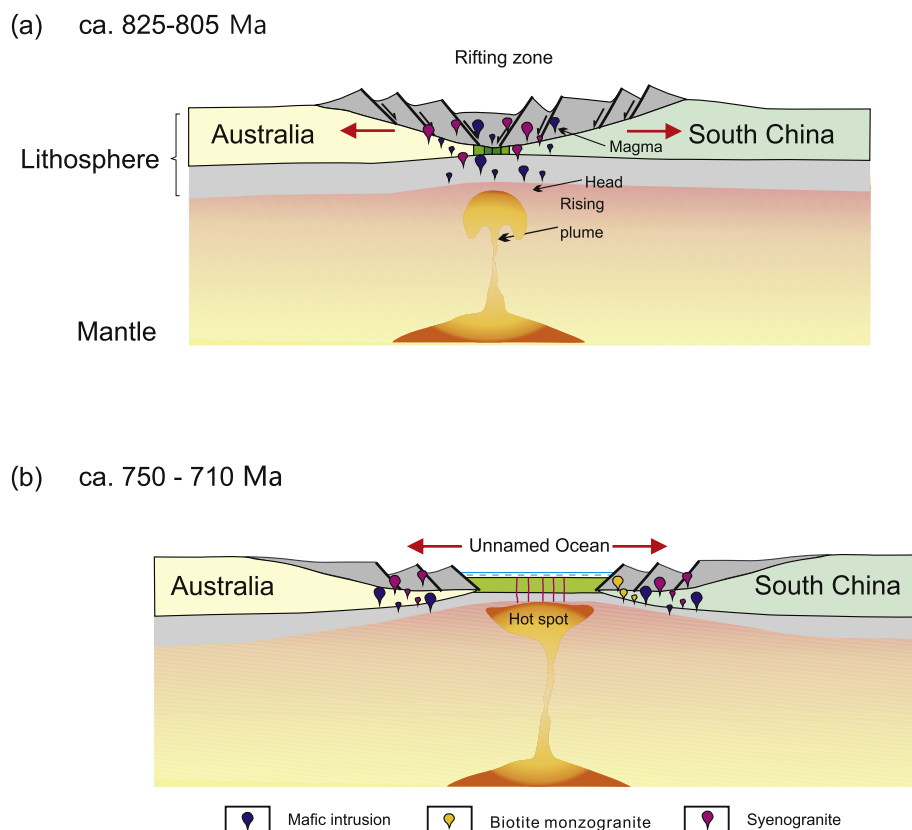


Fig. 14. Schematic cartoon showing the early Neoproterozoic tectonic evolution of eastern South China.

6. Conclusion

Detailed and new geochronological, geochemical and Nd–Hf–O isotopic data are presented in this contribution. These data leads to the following salient findings about the origin and tectonic setting of the Dengganping Complex during the emplacement of granitic magma:

- (1) Magmatic zircons from granitic rocks in the Dengganping Complex yield U–Pb dates of ca. 815 Ma for a syenogranite and ca. 740 Ma for a biotite monzogranite. The syenogranite was emplaced in the initial stages of the Rodinia's fragmentation that started with the opening of an unnamed Proto-Tethyan Ocean at 825 Ma and continued until ca. 710 Ma.
- (2) The syenogranite area has an A2-type granite affinity, generated by partial melting of a Paleo- to Mesoproterozoic crustal source. The emplacement of the biotite monzogranite is derived from partial melting of a late Mesoproterozoic to early Neoproterozoic crust by upwelling of mafic material.
- (3) The $\delta^{18}\text{O}$ value for zircon from the ca. 740 Ma biotite monzogranite is indicative of a rift setting with its protolith experienced high-temperature water–rock interactions generating low-oxygen isotopic values.

From the data collected for this study, the granitic plutons in the Dengganping Complex are here interpreted as part of a ca. 825–710 Ma magmatic event forming a widespread curvilinear zone along western to northern Yangtze Block. The magmatism is associated with rifting powered by a mantle plume in a within-plate tectonic setting, rather than being volcanic-arc granites emplaced along Longmenshan Fault Zone.

Declaration of competing interest

The authors declare that they have no known competing financial interests or personal relationships that could have appeared to influence the work reported in this paper.

Acknowledgements

Authors thank the Editor-in-Chief Michael Roden and two anonymous referees for their helpful comments. The National Natural Science Foundation of China (41702108), China Postdoctoral Science Foundation (2019M650833), Open Fund Project of State Key Laboratory of Lithospheric Evolution (SKL-K201902), Open Fund Project of State Key Laboratory for Mineral Deposits Research (2019-LAMD-K14) and Everest Scientific Research Program of Chengdu University of Technology financially supported this study. The authors are grateful to Dr Jing-Ji Li for help in the field work, Prof. Xian-Hua Li for constructive comments, Dr Qiang Zhang for assistance during LA-MC-ICP-MS analyses, and Prof. Qiu-Li Li, Hong-Xia Ma, Xiao-Xiao Ling, Jiao Li, Yu Liu and Guo-Qiang Tang for their help during SIMS analyses.

Appendix A. Supplementary data

Supplementary data to this article can be found online at <https://doi.org/10.1016/j.lithos.2020.105602>.

References

- Allègre, C.J., Minster, J.F., 1978. Quantitative models of trace element behavior in magmatic processes. *Earth Planet. Sci. Lett.* 38 (1), 1–25. [https://doi.org/10.1016/0012-821X\(78\)90123-1](https://doi.org/10.1016/0012-821X(78)90123-1).
- Amelin, Y., Lee, D.C., Halliday, A.N., 2000. Early-middle Archaean crustal evolution deduced from Lu-Hf and U-Pb isotopic studies of single zircon grains. *Geochim. Cosmochim. Acta* 64 (24), 4205–4225. [https://doi.org/10.1016/S0016-7037\(00\)00493-2](https://doi.org/10.1016/S0016-7037(00)00493-2).
- Ao, H.W., Zhang, Y.K., Zhang, R.Y., Zhang, Y., Sun, Y., 2014. Neoproterozoic crust tectonics on the northern margin of the Yangtze: Granite geochemistry, zircon LA-ICP-MS U-Pb geochronology and Hf isotope evidence from the Zu Shidian field of South China. *Geol. Rev.* 60 (6), 1393–1408 (in Chinese with English abstract).
- Atherton, M.P., Petford, N., 1993. Generation of sodium-rich magmas from newly underplated basaltic crust. *Nature* 362 (6416), 144–146. <https://doi.org/10.1038/362144a0>.
- Barbarin, B., 1999. A review of the relationships between granitoid types, their origins and their geodynamic environments. *Lithos* 46 (3), 605–626. [https://doi.org/10.1016/S0024-4937\(98\)00085-1](https://doi.org/10.1016/S0024-4937(98)00085-1).
- Belousova, E.A., Griffin, W.L., O'Reilly, S.Y., 2006. Zircon morphology, trace element signatures and Hf-isotope composition as a tool for petrogenetic modeling: examples from eastern Australian granitoids. *J. Petrol.* 47, 329–353.
- Bindeman, I.N., Valley, J.W., 2002. Oxygen isotope study of the Long Valley magma system, California: isotope thermometry and convection in large silicic magma bodies. *Contrib. Mineral. Petrol.* 144, 185–205.
- Bindeman, I.N., Davis, A.M., Drake, M.J., 1998. Ion microprobe study of plagioclase–basalt partition experiments at natural concentration levels of trace elements. *Geochim. Cosmochim. Acta* 62, 1175–1193.
- Bindeman, I.N., Fu, B., Kita, N.T., Valley, J.W., 2008. Origin and evolution of silicic magmatism at Yellowstone based on ion microprobe analysis of isotopically zone zircons. *J. Petrol.* 49, 163–193. <https://doi.org/10.1093/petrology/egm075>.
- Breiter, K., Škoda, R., 2017. Zircon and whole-rock Zr/Hf ratios as markers of the evolution of granitic magmas: examples from the Teplice caldera (Czech Republic/Germany). *Mineral. Petrol.* 111 (4), 435–457.
- Breiter, K., Lamarao, C.N., Kras Borges, R.M., Dall'Agnol, R., 2014. Chemical characteristics of zircon from A-type granites and comparison to zircon of S-type granites. *Lithos* 192, 198–225.
- Burchfiel, B., Chen, Z.L., Liu, Yipin, Royden, L.H., 1995. Tectonics of the Longmen Shan and adjacent regions, Central China. *Int. Geol. Rev.* 37 (8), 661–735. <https://doi.org/10.1080/00206819509465424>.
- Cawood, P.A., Pisarevsky, S.A., 2017. Laurentia-Baltica-Amazônia relations during Rodinia assembly. *Precambrian Res.* 292, 386–397.
- Cawthorn, R.G., Strong, D.F., Brown, P.G., 1976. Origin of corundum-normative intrusive and extrusive magmas. *Nature* 259, 102–104. <https://doi.org/10.1038/259102a0>.
- Chappell, B.W., 1999. Aluminium saturation in I-and S-type granites and the characterization of fractionated haplogranites. *Lithos* 46 (3), 535–551.
- Chappell, B.W., White, A.J.R., 1974. Two contrasting granite type. *Pac. Geol.* 8, 173–174.
- Chappell, B.W., White, A.J.R., 1992. I-and S-type granites in the Lachlan Fold Belt. *Earth Environ. Sci. Trans. Royal Soc. Edinb.* 83 (1–2), 1–26.
- Chen, Y.L., Luo, Z.H., Zhao, J.X., Li, Z.H., Zhang, H.F., Song, X., 2004. The origin of the Kangding complex of Suining, Sichuan, based on zircon SHRIMP age and petrogeochemical characteristics. *Sci. China D* 34 (8), 687–697. <https://doi.org/10.1360/zd2004-34-8-687> (in Chinese with English abstract).
- Chen, Z.G., Zhang, L.C., Wu, H.Y., Wan, B., Zeng, Q.D., 2008. Geochemical and tectonic setting of A-type granites in the Nianziguoyu molybdenum deposit, Xilalumulin metallogenetic belt, Inner Mongolia. *Acta Petrol. Sin.* 24 (4), 257–267 (in Chinese with English abstract).
- Chung, S.L., Liu, D., Ji, J., Chu, M.F., Lee, H.Y., Wen, D.J., Zhang, Q., 2003. Adakites from continental collision zones: melting of thickened lower crust beneath southern Tibet. *Geology* 31 (11), 1021–1024. <https://doi.org/10.1130/G19796.1>.
- Collins, W.J., Beams, S.D., White, A.J.R., Chappell, B.W., 1982. Nature and origin of A-type granites with particular reference to southeastern Australia. *Contrib. Mineral. Petrol.* 80 (2), 189–200. <https://doi.org/10.1007/BF00374895>.
- Condie, K.C., 2001. Continental Growth during formation of Rodinia at 1.35–0.9 Ga. *Gondwana Res.* 4 (1), 5–16. [https://doi.org/10.1016/S1342-937X\(05\)70650-X](https://doi.org/10.1016/S1342-937X(05)70650-X).
- Cui, X., Jiang, X., Wang, J., Zhuo, J., Xiong, G., Lu, J., Deng, Q., Wu, H., Liu, J., 2013. Zircon U-Pb Geochronology for the Stratotype Section of the Neoproterozoic Chengjiang Formation in Central Yunnan and Its Geological Significance. *Geosci.* 27, 547–556 (in Chinese with English abstract).
- Cui, X., Jiang, X., Wang, J., Zhuo, J., Deng, Q., Wei, Y., 2015. Mid-Neoproterozoic diabase dykes from Xide in the western Yangtze Block, South China: new evidence for continental rifting related to the breakup of Rodinia supercontinent. *Precambrian Res.* 268, 339–356. <https://doi.org/10.1016/j.precamres.2015.07.017>.
- Dalziel, I.W.D., 1991. Pacific margins of Laurentia and East Antarctica–Australia as a conjugate rift pair: evidence and implications for an Eocambrian supercontinent. *Geology* 19 (6), 598–601.
- Deng, Q., Wang, J., Wang, Z., Jiang, X., Du, Q., Wu, H., Yang, F., Cui, X., 2013. Zircon U-Pb Ages for Tuffs from the Dashigou and Sanlangpu Formations of the Xixiang Group in the Northern Margin of Yangtze Block and Their Geological Significance. *J. Jilin Jianzhu Univ. Earth Sci.* Ed. 43, 797–808,819 (in Chinese with English abstract).
- Dong, Y., Santosh, M., 2016. Tectonic architecture and multiple orogeny of the Qinling Orogenic Belt, Central China. *Gondwana Res.* 29 (1), 1–40. <https://doi.org/10.1016/j.gr.2015.06.009>.
- Dong, Y., Liu, X., Santosh, M., Zhang, X., Chen, Q., Yang, C., Yang, Z., 2011. Neoproterozoic subduction tectonics of the northwestern Yangtze Block in South China: Constraints from zircon U-Pb geochronology and geochemistry of mafic intrusions in the Hannan Massif. *Precambrian Res.* 189, 66–90.
- Dong, Y., Liu, X., Santosh, M., Chen, Q., Zhang, X., Li, W., Zhang, G., 2012. Neoproterozoic accretionary tectonics along the northwestern margin of the Yangtze Block, China: constraints from zircon U-Pb geochronology and geochemistry. *Precambrian Res.* 196, 247–274. <https://doi.org/10.1016/j.precamres.2011.12.007>.
- Dong, Y., Sun, S., Yang, Z., Liu, X., Zhang, F., Li, W., Cheng, B., He, D., Zhang, G., 2017. Neoproterozoic subduction-accretionary tectonics of the South Qinling Belt, China. *Precambrian Res.* 293, 73–90.
- Du, L.L., Qin, Y.S., Yang, C.H., Wang, X.S., Zhou, X.W., Ren, L.D., Yang, Z.S., 2007. Reconsideration of the Kangding Group on the western edge of the Yangtze Platform: (in Chinese with English abstract).

- evidence from geochemistry and chronology. *Acta Geol. Sin.* 81 (11), 1562–1577 (in Chinese with English abstract).
- Du, LL., Guo, J.H., Nutman, A.P., Wyman, D., Geng, Y.S., Yang, C.H., Liu, F.L., Ren, L.D., Zhou, X.W., 2014. Implications for Rodinia reconstructions for the initiation of Neoproterozoic subduction at ~860 Ma on the western margin of the Yangtze Block: Evidence from the Guandaoshan Pluton. *Lithos* 196–197, 67–82. <https://doi.org/10.1016/j.lithos.2014.03.002>.
- Eby, G.N., 1992. Chemical subdivision of the A-type granitoids: petrogenetic and tectonic implications. *Geology* 20 (7), 641–644. [https://doi.org/10.1130/0091-7613\(1992\)020<0641:CSOTAT>2.3.CO;2](https://doi.org/10.1130/0091-7613(1992)020<0641:CSOTAT>2.3.CO;2).
- Frost, B.R., Barnes, C.G., Collins, W.J., Arculus, R.J., Ellis, D.J., Frost, C.D., 2001. A geochemical classification for granitic rocks. *J. Petrol.* 42 (11), 2033–2048. <https://doi.org/10.1093/petrology/42.11.2033>.
- Gan, B.P., Lai, S.C., Qin, J.F., Zhu, R.Z., Zhao, S.W., Li, T., 2017. Neoproterozoic alkaline intrusive complex in the northwestern Yangtze Block, Mican Mountains region, South China: petrogenesis and tectonic significance. *Int. Geol. Rev.* 59, 311–332.
- Gao, P., Zheng, Y.F., Zhao, Z.F., 2016. Distinction between S-type and peraluminous I-type granites: Zircon versus whole-rock geochemistry. *Lithos* 258–259, 77–91.
- Gao, Y.Y., Li, X.H., Griffin, W.L., O'Reilly, S.Y., Wang, Y.F., 2014. Screening criteria for reliable U-Pb geochronology and oxygen isotope analysis in uranium-rich zircons: a case study from the Suzhou A-type granites, SE China. *Lithos* 192, 180–191. <http://dx.doi.org/10.1016/j.lithos.2014.02.002>.
- Geng, Q., Wang, L., Pan, G., Jin, Z., Zhu, D., Liao, Z., Li, G., Li, F., 2007. Volcanic rock geochemistry and tectonic implication of the Luobadui Formation on the Gangdese zone, Xizang (Tibet). *Acta Petrol. Sin.* 23, 2699–2714.
- Geng, Y., Yang, C., Wang, X., Ren, L., Zhou, X., Wang, Y., Yang, Z., Yang, Z., 2006. The stipulation of Neoproterozoic TFG in western Yangtze block and its significance. *Acta Petrol. Mineral.* 25, 273–281 (in Chinese with English abstract).
- Geng, Y.Y., 2010. Study on the Dating and Geochemical Characteristics of the SHRIMP Zircon U-Pb Granites on the Northern Margin of the Yangtze Block. (Master's Thesis). China University of Geosciences (Beijing), Beijing (in Chinese with English abstract).
- Griffin, W.L., Pearson, N.J., Belousova, E., Jackson, S.E., van Achterbergh, E., O'Reilly, S.Y., Shee, S.R., 2000. The Hf isotope composition of cratonic mantle: LAM-MC-ICPMS analysis of zircon megacrysts in kimberlites. *Geochim. Cosmochim. Acta* 64, 133–147. [https://doi.org/10.1016/S0016-7037\(99\)00343-9](https://doi.org/10.1016/S0016-7037(99)00343-9).
- Grimes, C.B., Wooden, J.L., Cheadle, M.J., John, B.E., 2015. "Fingerprinting" tectonomagmatic provenance using trace elements in igneous zircon. *Contrib. Mineral. Petrol.* 170 (5–6), 1–26.
- Gu, Z., Wang, Z., 2014. The discovery of Neoproterozoic extensional structures and its significance for gas exploration in the Central Sichuan Block, Sichuan Basin, South China. *Sci. China Earth Sci.* 57, 2758–2768.
- Guo, C.L., Wang, D.H., Chen, Y.C., Zhao, Z.G., Wang, Y.B., Fu, X.F., Fu, D.M., 2007. SHRIMP U-Pb zircon ages and major element, trace element and Nd-Sr isotope geochemical studies of a Neoproterozoic granitic complex in western Sichuan: Petrogenesis and tectonic significance. *Acta Petrol. Sin.* 23, 2457–2470 (in Chinese with English abstract).
- Harlan, S.S., Heaman, L., LeCheminant, A.N., Premo, W.R., 2003. Gunbarrel mafic magmatic event: a key 780 Ma time marker for Rodinia plate reconstructions. *Geology* 31, 1053–1056.
- Harris, C., Ashwal, L.D., 2002. The origin of low $\delta^{18}\text{O}$ granites and related rocks from the Seychelles. *Contrib. Mineral. Petrol.* 143, 366–376. <https://doi.org/10.1007/s00410-002-0349-6>.
- He, D., Li, D., Li, C., Li, Y., Mei, Q., 2017. Neoproterozoic rifting in the Upper Yangtze Continental Block: Constraints from granites in the Well W117 borehole. *South China. Sci. Rep.* 7 (1). <https://doi.org/10.1038/s41598-017-12764-y>.
- He, J.M., Chen, G.H., Yang, Z.L., 1988. Kang-Dian grey gneiss. Chongqing Press (in Chinese).
- Hoffman, P.F., 1991. Did the breakout of Laurentia turn Gondwanaland inside-out? *Science* 252, 1409–1412.
- Hoskin, P.W., Schaltegger, U., 2003. The composition of zircon and igneous and metamorphic petrogenesis. *Rev. Mineral. Geochem.* 53 (1), 27–62.
- Hu, J., 2013. Study on metamorphism and geochronology of the Douling Complex, South Qinling orogen (Master's Thesis). Chinese Academy of Geological Sciences, Beijing (in Chinese with English abstract).
- Huang, D.L., Wang, X.L., Xia, X.P., Wan, Y.S., Zhang, F.F., Li, J.Y., Du, D.H., 2019. Neoproterozoic low- $\delta^{18}\text{O}$ zircons revisited: implications for Rodinia configuration. *Geophys. Res. Lett.* 46, 678–688. <https://doi.org/10.1029/2018GL081117>.
- Huang, T.K., Chen, B.W., 1987. *The Evolution of the Tethys in China and Adjacent Regions*. Geological Publ. House, Beijing (in Chinese).
- Huang, X.L., Xu, Y.G., Li, X.H., Li, W.X., Lan, J.B., Zhang, H.H., Yang, Q.J., 2008. Petrogenesis and tectonic implications of Neoproterozoic, highly fractionated A-type granites from Mianning, South China. *Precambrian Res.* 165 (3–4), 190–204. <https://doi.org/10.1016/j.precamres.2008.06.010>.
- Huang, X.L., Xu, Y.G., Lan, J.B., Yang, Q.J., Luo, Z.Y., 2009. Neoproterozoic adakitic rocks from Mopanshan in the Western Yangtze craton: Partial melts of a thickened lower crust. *Lithos* 112, 367–381. <https://doi.org/10.1016/j.lithos.2009.03.028>.
- Huppert, H.E., Stephen, R., Sparks, J., 1985. Cooling and contamination of mafic and ultramafic magmas during ascent through continental crust. *Earth Planet. Sci. Lett.* 74 (4), 371–386.
- Jiang, N., Chen, J.Z., Guo, J.H., Chang, G.H., 2012. In situ zircon U-Pb, oxygen and hafnium isotopic compositions of Jurassic granites from the North China craton: Evidence for Triassic subduction of continental crust and subsequent metamorphism-related ^{18}O depletion. *Lithos* 142–143, 84–94.
- Jiang, Z.F., Cui, X.Z., Jiang, X.S., Wang, J., Zhuo, J.W., Xiong, G.Q., Lu, J.Z., Wu, H., Wei, Y.N., 2016. New zircon U-Pb ages of the pre-Sturtian rift successions from the western Yangtze Block, South China and their geological significance. *Int. Geol. Rev.* 58, 1064–1075.
- Lai, S.C., Qin, J.F., Zhu, R.Z., Zhao, S.W., 2015. Neoproterozoic quartz monzonodiorite-granodiorite association from the Luding-Kangding area: Implications for the interpretation of an active continental margin along the Yangtze Block (South China Block). *Precambrian Res.* 267, 196–208.
- Li, J.Y., Wang, X.L., Gu, Z.D., 2018. Petrogenesis of the Jiaozidong granitoids and associated basaltic porphyries: Implications for extensive early Neoproterozoic arc magmatism in western Yangtze Block. *Lithos* 296, 547–562.
- Li, M., 2003. Study on the geochemistry of granitoid intrusives of Douling Group in the east Qinling and its geological significance (Master's Thesis). Northwest University, Xi'an (in Chinese with English abstract).
- Li, Q.W., Zhao, J.H., 2016. Petrogenesis of the Wudang mafic dikes: Implications of changing tectonic settings in South China during the Neoproterozoic.
- Li, Q.W., Zhao, J.H., 2018. The Neoproterozoic high-Mg dioritic dikes in South China formed by high pressures fractional crystallization of hydrous basaltic melts. *Precambrian Res.* 309, 198–211.
- Li, X., Qi, C.H., Liu, Y., Liang, X.R., Tu, X.L., Xie, L.W., Yang, Y.H., 2005. Petrogenesis of the Neoproterozoic bimodal volcanic rocks along the western margin of the Yangtze Block: New constraints from Hf isotopes and Fe/Mn ratios. *Chin. Sci. Bull.* 21, 2481–2486.
- Li, X.H., 1999. U-Pb zircon ages of granites from the southern margin of the Yangtze Block: timing of Neoproterozoic Jinning: Orogeny in SE China and implications for Rodinia Assembly. *Precambrian Res.* 97 (1–2), 43–57. [https://doi.org/10.1016/S0301-9268\(99\)00020-0](https://doi.org/10.1016/S0301-9268(99)00020-0).
- Li, X.H., Li, Z.X., Zhou, H.W., Liu, Y., Liang, X.R., 2002a. Zircon U-Pb geochronology, element and Nd isotopic study of Neoproterozoic basaltic magmatic rocks in Western Sichuan: petrogenesis and geodynamic implications. *Geosci. Front.* 9 (4), 329–338 (in Chinese with English abstract).
- Li, X.H., Li, Z.X., Zhou, H., Liu, Y., Kinny, P.D., 2002b. U-Pb zircon geochronology, geochemistry and Nd isotopic study of Neoproterozoic bimodal volcanic rocks in the Kangdian Rift of South China: implications for the initial rifting of Rodinia. *Precambrian Res.* 113 (1–2), 135–154. [https://doi.org/10.1016/S0301-9268\(01\)00207-8](https://doi.org/10.1016/S0301-9268(01)00207-8).
- Li, X.H., Li, Z.X., Ge, W., Zhou, H., Li, W., Liu, Y., Wingate, M.T., 2003a. Neoproterozoic granitoids in South China: crustal melting above a mantle plume at ca. 825 Ma? *Precambrian Res.* 122 (1–4), 45–83. [https://doi.org/10.1016/S0301-9268\(02\)00207-3](https://doi.org/10.1016/S0301-9268(02)00207-3).
- Li, X.H., Li, Z.X., Zhou, H.W., Liu, Y., Liang, X.R., Li, W.X., 2003b. SHRIMP zircon U-Pb age, elemental and Nd isotopic geochemistry of the Guanshanshan rock mass in southwestern Sichuan Province-petrogenetic and tectonic implications. *Sci. China D* 32 (S2), 60–68 (in Chinese with English abstract).
- Li, X.H., Li, Z.X., Wingate, M.T., Chung, S.L., Liu, Y., Lin, G.C., Li, W.X., 2006. Geochemistry of the 755 Ma Mundine Well dyke swarm, northwestern Australia: part of a Neoproterozoic mantle superplume beneath Rodinia? *Precambrian Res.* 146 (1–2), 1–15. <https://doi.org/10.1016/j.precamres.2005.12.007>.
- Li, X.H., Zhu, W.G., Zhong, H., Wang, X.C., He, D.F., Bai, Z.J., Liu, F., 2010. The Tongde Picritic Dikes in the Western Yangtze Block: evidence for ca. 800-Ma mantle plume magmatism in South China during the breakup of Rodinia. *J. Geol.* 118 (5), 509–522. <https://doi.org/10.1086/655113>.
- Li, X.H., Li, W.X., He, B., 2012. Formation of the South China Land Block and Rodinia Supercontinent polymerization-pyrolysis-observation, interpretation, and inspection. *Bull. Mineral. Petrol.* 31 (6), 543–559 (in Chinese with English abstract).
- Li, Z.X., 1995. South China in Rodinia: part of the missing link between Australia-East Antarctica and Laurentia. *Geology* 23 (5), 407–410. [https://doi.org/10.1130/0091-7613\(1995\)023<407:SCRPO>2.3.CO;2](https://doi.org/10.1130/0091-7613(1995)023<407:SCRPO>2.3.CO;2).
- Li, Z.X., Powell, C.M., 2001. An outline of the palaeogeographic evolution of the Australasian region since the beginning of the Neoproterozoic. *Earth Sci. Rev.* 53 (3–4), 237–277.
- Li, Z.X., Zhang, L., Powell, C.M., 1995. South China in Rodinia: part of the missing link between Australia-East Antarctica and Laurentia? *Geol.* 23, 407–410.
- Li, Z.X., Zhang, L., Powell, C.M., 1996. Positions of the East Asian cratons in the Neoproterozoic supercontinent Rodinia. *Aust. J. Earth Sci.* 43 (6), 593–604. <https://doi.org/10.1080/0812009960872821>.
- Li, Z.X., Li, X.H., Kinny, P.D., Wang, J., Zhang, S., Zhou, H., 2003c. Geochronology of Neoproterozoic syn-rift magmatism in the Yangtze Craton, South China and correlations with other continents: evidence for a mantle superplume that broke up Rodinia. *Precambrian Res.* 122 (1–4), 85–109.
- Li, Z.X., Bogdanova, S.V., Collins, A.S., Davidson, A., De Waele, B., Ernst, R.E., Fitzsimons, I.C.W., Fuck, R.A., Gladkochub, D.P., Jacobs, J., Karlstrom, K.E., Lu, S., Natapov, L.M., Pease, V., Pisarevsky, S.A., Thrane, K., Vernikovsky, V., 2008. Assembly, configuration, and break-up history of Rodinia: a synthesis. *Precambrian Res.* 160, 179–210. <https://doi.org/10.1016/j.precamres>.
- Lin, G.C., Li, X.H., Li, W.X., 2007. SHRIMP U-Pb zircon age, geochemistry and Nd-Hf isotope of Neoproterozoic mafic dyke swarms in western Sichuan: petrogenesis and tectonic significance. *Sci. China D* 50 (1), 1–16. <https://doi.org/10.1007/s11430-007-2018-0>.
- Lin, M.B., Ma, Y.W., 1995. Discussion on the structural properties of Pengguan Complex in Longmen Mountain. *J. Chengdu Inst. Geol.* 16 (1), 42–46 (in Chinese with English abstract).
- Ling, W.L., Shan, B., Zhang, B.R., Li, H.M., Liu, Y., Cheng, J.P., 2003. Neoproterozoic tectonic evolution of the northwestern Yangtze craton, South China: implications for amalgamation and break-up of the Rodinia Supercontinent. *Precambrian Res.* 122, 111–140.
- Ling, W.L., Ren, B.F., Duan, R.C., Liu, X.M., Mao, X.W., Peng, L.H., Liu, Z.X., Cheng, J.P., Yang, H.M., 2007. Timing of the Wudangshan-Yaolining volcanic sequences and mafic sills in South Qinling: U-Pb zircon geochronology and tectonic implication. *Chin. Sci. Bull.* 53 (14), 2192–2199.
- Liu, H.Q., Xu, Y.G., He, B., 2013. Implications from zircon-saturation temperatures and lithological assemblages for early Permian thermal anomaly in Northwest China. *Lithos* 182–183, 125–133.

- Liu, J., Deng, J., Li, G., Xiao, C., Meng, F., Chen, F., Wu, W., Zhang, Q., 2017. Petrogenesis and tectonic significance of the Lianhuashan intrusion in the Lanping Basin, western Yunnan: Constraints from bulk element composition, zircon U-Pb geochronology and Hf isotopic compositions. *Acta Petrol. Sin.* 33, 2115–2128 (in Chinese with English abstract).
- Liu, J.B., Zhang, L.M., 2013. Neoproterozoic low to negative $\delta^{18}\text{O}$ volcanic and intrusive rocks in the Qinling Mountains and their geological significance. *Lithos* 230, 138–167.
- Liu, R., Zhang, B., Zhang, H., Yuan, H., 2009c. U-Pb zircon age, geochemical and Sr-Nd-Hf isotopic compositions of Neoproterozoic granitoids in northwestern margin of Yangtze block (South China): implications for Neoproterozoic tectonic evolution. *J. Earth Sci.* 20 (4), 659–680. <https://doi.org/10.1007/s12583-009-0058-4>.
- Liu, S.W., Yan, Q.R., Li, Q.G., Wang, Q.Z., 2009a. Genesis and tectonic significance of granitoids in the Kangding complex of the western margin of the Yangtze Craton. *Acta Petrol. Sin.* 25 (8), 1883–1896 (in Chinese with English abstract).
- Liu, S.W., Yang, Q., Li, Q.G., Wang, Q.Z., Yan, Q.R., 2009b. Petrogenetics of the Neoproterozoic Baoxing Complex and its constraints on the tectonic setting of the western margin of the Yangtze River. *Geosci. Front.* 16 (2), 107–118 (in Chinese with English abstract).
- Liu, Y., Shuguang, Li., Xiaofeng, G.U., 2006. Zircon SHRIMP U-Pb dating for olivine gabbro at Wangmuguan in the Beihuayang zone and its geological significance. *Sci. Bull.* 51, 2500–2506.
- Liu, Z.R., 2013. The Mineral Chemistry of the Neoproterozoic Hannan Acidic Complex in the Northwestern Margin of Yangzi (Master's Thesis): Wuhan. China University of Geosciences (in Chinese with English abstract).
- Liu, Z.R., Zhao, J.H., 2013. Mineralogical constraints on the origin of Neoproterozoic felsic intrusions, NW margin of the Yangtze Block, South China. *Int. Geol. Rev.* 55, 590–607.
- Loiselle, M.C., Wones, D.S., 1979. Characteristics and origin of Anorogenic granites. *Geol. Soc. Am. Abstr. Programs* 11, 468.
- Lu, J., Jiang, X., Wang, J., Zhuo, J., Xiong, G., Cui, X., 2013. SHRIMP zircon U-Pb age and its geological significance of Neoproterozoic Chengjiang Formation in Qiaojia Area, Northeast Yunnan. *J. Mineral. Petrol.* 33, 65–71 (in Chinese with English abstract).
- Luo, B.J., Liu, R., Zhang, H.F., Zhao, J.H., Yang, Y.H., Xu, W.C., Guo, L., Zhang, L.Q., Tao, L., Pan, F.B., Wang, W., Gao, Z., Shao, H., 2018. Neoproterozoic continental back-arc rift development in the Northwestern Yangtze Block: Evidence from the Hannan intrusive magmatism. *Gondwana Res.* 59, 27–42.
- Ma, Y.W., Wang, G.Z., Hu, X.W., 1996. Tectonic deformation characteristics of the "Peng irrigation complex rock" nappe. *Acta Geol. Sichuan* 2, 110–114 (in Chinese with English abstract).
- Maniar, P.D., Piccoli, P.M., 1989. Tectonic discrimination of granitoids. *Geol. Soc. Am. Bull.* 101 (5), 635–643. [https://doi.org/10.1130/0016-7606\(1989\)101<0635:TDOG>2.3.CO;2](https://doi.org/10.1130/0016-7606(1989)101<0635:TDOG>2.3.CO;2).
- McMenamin, M.A., McMenamin, D.L., 1990. *The Emergence of Animals: The Cambrian Breakthrough*. Columbia University Press ISBN 0-231-06647-3.
- Meng, E., Liu, F.L., Du, L.L., Liu, P.H., Liu, J.H., 2015. Petrogenesis and tectonic significance of the Baoxing granitic and mafic intrusions, southwestern China: Evidence from zircon U-Pb dating and Lu-Hf isotopes, and whole-rock geochemistry. *Gondwana Res.* 28, 800–815.
- Merdith, A.S., Collins, A.S., Williams, S.E., Pisarevsky, S., Foden, J.D., Archibald, D.B., Clark, C., 2017. A full-plate global reconstruction of the Neoproterozoic. *Gondwana Res.* 50, 84–134.
- Middlemost, E.A.K., 1985. *Magmas and Magmatic Rocks: An Introduction to Igneous Petrology*. Longmans, London.
- Middlemost, E.A.K., 1994. Naming materials in the magma/igneous rock system. *Earth-Sci. Rev.* 37 (3–4), 215–224. [https://doi.org/10.1016/0012-8252\(94\)90029-9](https://doi.org/10.1016/0012-8252(94)90029-9).
- Miller, C.F., McDowell, S.M., Mapes, R.W., 2003. Hot and cold granites? Implications of zircon saturation temperatures and preservation of inheritance. *Geology* 31, 529–532.
- Monani, S., Valley, J.W., 2001. Oxygen isotope ratios of zircon: magma genesis of low delta O-18 granites from the British Tertiary Igneous Province, western Scotland. *Earth Planet. Sci. Lett.* 184, 377–392.
- Moore, E.M., 1991. Southwest U.S.-East Antarctica (SWEAT) connection: a hypothesis. *Geology* 19 (5), 425–428. [https://doi.org/10.1130/0091-7613\(1991\)019<0425:SUEAS>2.3.CO;2](https://doi.org/10.1130/0091-7613(1991)019<0425:SUEAS>2.3.CO;2).
- Mu, C.L., Lin, S.L., Yu, Q., 2003. Age of U-Pb of Tianbaoshan formation in Sichuan Huili. *Stratigr.* 27 (3), 216–219 (in Chinese with English abstract).
- Munteanu, M., Wilson, A., Yao, Y., Harris, C., Chunnett, G., Luo, Y., 2010. The Tongde dioritic pluton (Sichuan, SW China) and its geotectonic setting: Regional implications of a local-scale study. *Gondwana Res.* 18, 455–465. <https://doi.org/10.1016/j.gr.2010.01.005>.
- Nie, S.Y., Yin, A., Rowley, D.B., Jin, Y., 1994. Exhumation of the Dabie Shan ultra-high-pressure rocks and accumulation of the Songpan-Ganzi flysch sequence, Central China. *Geology* 22, 999–1002.
- Park, J.K., Buchan, K.L., Harlan, S.S., 1995. A proposed giant radiating dyke swarm formed by the separation of Laurentia and Australia based on paleomagnetism of ca. 780 Ma mafic intrusions in western North America. *Earth Planet. Sci. Lett.* 132, 129–139. [https://doi.org/10.1016/0012-821X\(95\)00059-L](https://doi.org/10.1016/0012-821X(95)00059-L).
- Pearce, J.A., Harris, N.B.W., Tindle, A.G., 1984. Trace Element Discrimination Diagrams for the tectonic interpretation of granitic rocks. *J. Petrol.* 25 (4), 956–983. <https://doi.org/10.1093/petrology/25.4.956>.
- Peccerillo, A., Taylor, S.R., 1976. Geochemistry of Eocene calc-alkaline volcanic rocks from the Kastamonu area, northern Turkey. *Contrib. Mineral. Petroil.* 58 (1), 63–81. <https://doi.org/10.1007/BF00384745>.
- Pei, X.Z., Ding, S.P., Li, Z.C., Li, R.B., Feng, J.Y., Sun, Y., Liu, Z.Q., 2009. The SHRIMP U-Pb ages of the zircons from the Neoproterozoic granites of the Jiaozidong orogenic belt in the Longmenshan orogenic belt. *J. Northwest Univ. (Sci. Ed.)* 39 (3), 425–433 (in Chinese with English abstract).
- Powell, C.M., Li, Z.X., McElhinny, M.W., Meert, J.G., Park, J.K., 1993. Paleomagnetic constraints on timing of the Neoproterozoic breakup of Rodinia and the Cambrian formation of Gondwana. *Geology* 21 (10), 889–892.
- Ren, C., Pang, W., Sun, Z., Yin, F., 2013. Zircon SHRIMP U-Pb dating of basalt from Huangshuihe Group on the western margin of the Yangtze block and its geological significance. *Geol. China* 40, 1007–1015 (in Chinese with English abstract).
- Rubatto, D., 2002. Zircon trace element geochemistry: partitioning with garnet and the link between U-Pb ages and metamorphism. *Chem. Geol.* 184 (1–2), 123–138. [https://doi.org/10.1016/S0009-2541\(01\)00355-2](https://doi.org/10.1016/S0009-2541(01)00355-2).
- She, Z., Ma, C., Mason, R., Li, J., Wang, G., Lei, Y., 2006. Provenance of the Triassic Songpan-Ganzi flysch, West China. *Chem. Geol.* 231 (1–2), 159–175.
- SPBGMR (Sichuan Provincial Bureau of Geology and Mineral Resources), 1991. *Regional Geological of Sichuan Province*. Geological Publishing House, Beijing (in Chinese).
- Spencer, C.J., Cavosie, A.J., Raub, T.D., Rollinson, H., Jeon, H., Searle, M.P., 2017. Evidence for melting mud in Earth's mantle from extreme oxygen isotope signatures in zircon. *Geology* 45, 975–978. <https://doi.org/10.1130/G39402.1>.
- Sun, J., Shu, L., Santosh, M., Wang, L., 2017. Neoproterozoic tectonic evolution of the Jiuling terrane in the central Jiangnan orogenic belt (South China): Constraints from magmatic suites. *Precambrian Res.* 302, 279–297.
- Sun, S.S., McDonough, W.F., 1989. Chemical and isotopic systematics of oceanic basalts: implications for mantle composition and processes. *Geol. Soc. Lond. Spec. Publ.* 42 (1), 313–345.
- Tian, H., Li, H.K., Zhou, H.Y., Zhang, J., Zhang, K., Yu, J.Z., Xin, L.S., 2017. The sedimentary age of the Huashan Group on the northern margin of the Yangtze plate and its constraint on the cracking of the Rodinia supercontinent. *Acta Geol. Sin.* 91 (11), 2387–2408 (in Chinese with English abstract).
- Torsvik, T.H., 2003. The Rodinia jigsaw puzzle. *Science* 300 (5624), 1379–1381. <https://doi.org/10.1126/science.1083469>.
- Tucker, R.D., Ashwal, L.D., Torsvik, T.H., 2001. U-Pb geochronology of Seychelles granitoids: a Neoproterozoic continental arc fragment. *Earth Planet. Sci. Lett.* 187, 27–38. [https://doi.org/10.1016/s0012-821x\(01\)00282-5](https://doi.org/10.1016/s0012-821x(01)00282-5).
- Valentine, J.W., Moores, E.M., 1970. Plate-tectonic regulation of faunal diversity and sea level: a Model. *Nature* 228, 657–659. <https://doi.org/10.1038/228657a0>.
- Valley, J.W., Kinny, P.D., Schulze, D.J., Spicuzza, M.J., 1998. Zircon megacrysts from kimberlite: oxygen isotope variability among mantle melts. *Contrib. Mineral. Petroil.* 133, 1–11.
- Valley, J.W., Bindeman, I.N., Peck, W.H., 2003. Empirical calibration of oxygen isotope fractionation in zircon. *Geochim. Cosmochim. Acta* 67, 3257–3266.
- Valley, J.W., Lackey, J.S., Cavosie, A.J., Clechenko, C.C., Spicuzza, M.J., Basei, A.S., Bindeman, I.N., 2005. 4.4 billion years of crustal maturation: oxygen isotope ratios of magmatic zircon. *Mineral. Petroil.* 150, 561–580. <https://doi.org/10.1007/s00410-005-0025-8>.
- Wan, B., Wu, F., Chden, L., Zhao, L., Liang, X., Xiao, W., Zhu, R., 2019. Cyclical one-way continental rupture-drift in the Tethyan evolution: subduction-driven plate tectonics. *Sci. China Earth Sci.* 62 (12), 2005–2016.
- Wang, J., 2000. Evolution of the Neoproterozoic Rift Basin in South China: Concurrently on the Relationship with Rodinia Disintegration. Geological Publishing House, Beijing (in Chinese with English abstract).
- Wang, J., Li, Z.X., 2003. History of Neoproterozoic rift basins in South China: implications for Rodinia break-up. *Precambrian Res.* 122 (1), 141–158. [https://doi.org/10.1016/S0301-9268\(02\)00209-7](https://doi.org/10.1016/S0301-9268(02)00209-7).
- Wang, L.J., Yu, J.H., Griffin, W.L., O'Reilly, S.Y., 2012. Early crustal evolution in the western Yangtze Block: evidence from U-Pb and Lu-Hf isotopes on detrital zircons from sedimentary rocks. *Precambrian Res.* 222–223, 368–385. <https://doi.org/10.1016/j.precamres.2011.08.001>.
- Wang, L.J., Griffin, W.L., Yu, J.H., O'Reilly, S.Y., 2013b. U-Pb and Lu-Hf isotopes in detrital zircon from Neoproterozoic sedimentary rocks in the northern Yangtze Block: implications for Precambrian crustal evolution. *Gondwana Res.* 23, 1261–1272. <https://doi.org/10.1016/j.gr.2012.04.013>.
- Wang, M.X., Nebel, O., Wang, C.Y., 2016. The flaw in the crustal 'Zircon Archive': mixed Hf isotope signatures record progressive contamination of late-stage liquid in mafic-ultramafic layered intrusions. *J. Petrol.* 57, 27–52.
- Wang, Q., Derek, A.W., Li, Z.X., Bao, Z.W., Zhao, Z.H., Wang, Y.W., Jian, P., Yang, Y.H., Chen, L.L., 2010. Petrology, geochronology and geochemistry of ca. 780 Ma A-type granites in South China: Petrogenesis and implications for crustal growth during the breakup of the supercontinent Rodinia. *Precambrian Res.* 178, 185–208.
- Wang, W., Cawood, P.A., Zhou, M.F., Pandit, M.K., Xia, X.P., Zhao, J.H., 2017a. Low- $\delta^{18}\text{O}$ Rhylolites from the Malani Igneous Suite: a positive Test for South China and NW India Linkage in Rodinia. *Geophys. Res. Lett.* 44 (20), 10298–10305. <https://doi.org/10.1002/2017GL074717>.
- Wang, X.C., Li, X.H., Li, W.X., Li, Z.X., Liu, Y., Yang, Y.H., Liang, X.R., Tu, X.L., 2008. The Bikou basalts in the northwestern Yangtze block, South China: Remnants of 820–810 Ma continental flood basalts? *Geol. Soc. Am. Bull.* 120, 1478–1492.
- Wang, X.C., Li, Z.X., Li, X.H., Li, Q.L., Zhang, Q.R., 2011. Geochemical and Hf-Nd isotope data of Nanhua rift sedimentary and volcanoclastic rocks indicate a Neoproterozoic continental flood basalts provenance. *Lithos* 127, 427–440.
- Wang, X.L., Zhou, J.C., Qiu, J.S., Zhang, W.L., Liu, X.M., Zhang, G.L., 2006. LA-ICP-MS U-Pb zircon geochronology of the Neoproterozoic igneous rocks from Northern Guangxi, South China: Implications for tectonic evolution. *Precambrian Res.* 145, 111–130.
- Wang, X.L., Zhou, J.C., Wan, Y.S., Kitajima, K., Wang, D., Bonamici, C., Qiu, S.Q., Sun, T., 2013. Magmatic evolution and crustal recycling for Neoproterozoic strongly peraluminous granitoids from southern China: Hf and O isotopes in zircon. *Earth Planet. Sci. Lett.* 366, 71–82. <https://doi.org/10.1016/j.epsl.2013.02.011>.
- Wang, X.L., Zhou, J.C., Chen, W., Zhang, F.F., Sun, X.M., 2017b. The formation and evolution of the Jiangnan Orogenic Belt. *Mineral. Petroil.* 36 (5), 714–735 (in Chinese with English abstract).

- Watts, K.E., Leeman, W.P., Bindeman, I.N., Larson, P.B., 2010. Supereruptions of the Snake River plain: two-stage derivation of low- $\delta^{18}\text{O}$ rhyolites from normal- $\delta^{18}\text{O}$ crust as constrained by Archean xenoliths. *Geology* 38, 503–506. <https://doi.org/10.1130/G30735.1>.
- Whalen, J.B., Currie, K.L., Chappell, B.W., 1987. A-type granites: geochemical characteristics, discrimination and petrogenesis. *Contrib. Mineral. Petrol.* 95 (4), 407–419. <https://doi.org/10.1007/BF00402202>.
- White, A.J.R., 1979. Sources of granite magmas. *Geol. Soc. Am. Abstr. Programs* 11, 539.
- White, A.J.R., Chappell, B.W., 1977. Ultrametamorphism and granitoid genesis. *Tectonophysics* 43, 7–22. [https://doi.org/10.1016/0040-1951\(77\)90003-8](https://doi.org/10.1016/0040-1951(77)90003-8).
- Whitehouse, M.J., Platt, J.P., 2003. Dating high-grade metamorphism—constraints from rare-earth elements in zircon and garnet. *Mineral. Petrol.* 145 (1), 61–74.
- Williams, I.S., Hergt, J.M., 2000. U-Pb dating of Tasmanian dolerites: a cautionary tale of SHRIMP analysis of high-U zircon. *Beyond 2000: New Frontiers in Isotope Geoscience Abstract Proceedings*. University of Melbourne, Australia, pp. 185–188.
- Wingate, M.T.D., Campbell, I.H., Compston, W., Gibson, G.M., 1998. Low microprobe U-Pb ages for Neoproterozoic-basaltic magmatism in south-Central Australia and implications for the breakup of Rodinia. *Precambrian Res.* 87, 135–159.
- Wu, F.Y., Jahn, B.M., Wilde, S.A., Lo, C.H., Yui, T.F., Lin, Q., Ge, W.C., Sun, D.Y., 2003. Highly fractionated I-type granites in NE China (I): geochronology and petrogenesis. *Lithos* 66, 241–273. [https://doi.org/10.1016/S0024-4937\(02\)00222-0](https://doi.org/10.1016/S0024-4937(02)00222-0).
- Wu, F.Y., Sun, D.Y., Jahn, B.M., Wilde, S., 2004. A Jurassic garnet-bearing granitic pluton from NE China showing tetrad REE patterns. *J. Asian Earth Sci.* 23, 731–744. [https://doi.org/10.1016/S1367-9120\(03\)00149-4](https://doi.org/10.1016/S1367-9120(03)00149-4).
- Wu, F.Y., Li, X.H., Yang, J.H., Zheng, Y.F., 2007a. Some problems in the study of granite genesis. *Acta Petrol. Sin.* 23 (6), 1217–1238 (in Chinese with English abstract).
- Wu, F.Y., Li, X.H., Yang, J.H., Zheng, Y.F., Gao, S., 2007b. Lu-Hf isotope system and its petrological application. *Acta Petrol. Sin.* 23 (2), 185–220 (in Chinese with English abstract).
- Wu, Y., Zhou, G., Gao, S., Liu, X., Qin, Z., Wang, H., Yang, S., 2014. Petrogenesis of Neoarchean TTG rocks in the Yangtze Craton and its implication for the formation of Archean TTGs. *Precambrian Res.* 254, 73–86.
- Xiao, L., Zhang, H.F., Ni, P.Z., Xiang, H., Liu, X.M., 2007. LA-ICP-MS U-Pb zircon geochronology of early Neoproterozoic mafic-intermediate intrusions from NW margin of the Yangtze Block, South China: Implication for tectonic evolution. *Precambrian Res.* 154, 221–235.
- Xiong, G., Jiang, X., Cui, X., Zhuo, J., Lu, J., Liu, J., Wang, Z., Wang, J., 2013. Strata location of the Lanbaoping Formation of the Proterozoic E'bian Group in the Western Yangtze Block and its chronological evidence of zircon SHRIMP U-Pb age. *Earth Sci. Front.* 20, 350–360.
- Xu, J.F., 2002. Origin of Mesozoic adakitic intrusive rocks in the Ningzhen area of East China: partial melting of delaminated lower continental crust? *Geology* 30 (12), 1111–1114. [https://doi.org/10.1130/0091-7613\(2002\)030<1111:OOMAHR>2.0.CO;2](https://doi.org/10.1130/0091-7613(2002)030<1111:OOMAHR>2.0.CO;2).
- Xu, X., Xia, L., Chen, J., Ma, Z., Li, X., Xia, Z., Wang, H., 2009. Zircon U-Pb dating and geochemical study of volcanic rocks from Sunjiahe Formation of Xixiang Group in northern margin of Yangtze Plate. *Acta Petrol. Sin.* 25, 3309–3326 (in Chinese with English abstract).
- Xu, Y., Yang, K.G., Polat, A., Yang, Z.N., 2016. The similar to 860 Ma mafic dikes and granitoids from the northern margin of the Yangtze Block, China: A record of oceanic subduction in the early Neoproterozoic. *Precambrian Res.* 275, 310–331.
- Xue, H., Ma, F., Song, Y., 2011. Geochemistry and SHRIMP zircon U-Pb data of Neoproterozoic meta-magmatic rocks in the Suizhou-Zaoyang area, northern margin of the Yangtze Craton, Central China. *Acta Petrol. Sin.* 27, 1116–1130 (in Chinese with English abstract).
- Yan, D.P., Zhou, M.F., Li, S.B., Wei, G.Q., 2011. Structural and geochronological constraints on the Mesozoic-Cenozoic tectonic evolution of the Longmen Shan thrust belt, eastern Tibetan Plateau. *Tecton.* 30 (6), 1–24. <https://doi.org/10.1029/2011TC002867>.
- Yan, M., Liu, S., Li, Q., Yang, P., Wang, W., Guo, R., Bai, X., Deng, Z., 2014. LA-ICP-MS zircon U-Pb chronology and Lu-Hf isotopic properties of the Mihunzhen pluton in the South Qinling tectonic belt. *Acta Petrol. Sin.* 30, 390–400 (in Chinese with English abstract).
- Yan, Q.R., Hanson, A.D., Wang, Z.Q., Druschke, P.A., Yan, Z., Wang, T., Liu, D.Y., Song, B., Pan, P., Zhou, H., Jiang, C.F., 2004. Neoproterozoic subduction and rifting on the northern margin of the Yangtze Plate, China: Implications for Rodinia reconstruction. *Int. Geol. Rev.* 46, 817–832.
- Yang, J.H., Wu, F.Y., Zhong, S.L., Luo, Q.H., 2008. Extensive geodynamic setting of the Early Cretaceous granite emplacement in the eastern part of North China: evidence from laser 40Ar/39Ar geochronology. *Acta Petrol. Sin.* 24 (6), 1175–1184 (in Chinese with English abstract).
- Yang, J.H., Liu, L., Liu, J., 2017. Research progress and prospects of diagenesis and mineralization in the Mesozoic Granite Province in South China. *Acta Petrol. Sin. J. Miner.* 37 (6), 791–800 (in Chinese with English abstract).
- Yang, P., Liu, S., Li, Q., Wang, Z., Wang, W., Bai, X., 2012a. Emplacing age of the Tiewadian Pluton in the South Qinling Tectonic Belt and its geological implications. *Acta Geol. Sin.* 86, 1525–1540 (in Chinese with English abstract).
- Yang, P.T., Liu, S.W., Li, Q.G., Wang, Z.Q., 2012b. Diagenesis times and geological significance of Tiewadian rock mass in the South Qinling Mountains. *Acta Geol. Sin.* 86 (9), 1525–1540 (in Chinese with English abstract).
- Yang, Y.N., Wang, X.C., Li, Q.L., Li, X.H., 2016. Integrated in situ U-Pb age and Hf-O analyses of zircon from Suixian group in northern Yangtze: new insights into the Neoproterozoic low- $\delta^{18}\text{O}$ magmas in the South China block. *Precambrian Res.* 273, 151–164. <https://doi.org/10.1016/j.precamres.2015.12.008>.
- Yao, W.H., Li, Z.X., Li, W.X., Li, X.H., Yang, J.H., 2014. From Rodinia to Gondwanaland: A tale of detrital zircon provenance analyses from the southern Nanhua basin, South China. *Am. J. Sci.* 314, 278–313.
- Yuan, F., Liu, J.J., Carranza, E.J.M., Zhang, S., Zhai, D.G., Liu, G., Wang, G.W., Zhang, H.Y., Sha, Y.Z., Yang, S.-S., 2018. Zircon trace element and isotopic (Sr, Nd, Hf, Pb) effects of assimilation-fractional crystallization of pegmatite magma: A case study of the Guangshigou biotite pegmatites from the North Qinling Orogen, central China. *Lithos* 302, 20–36.
- Zhang, P., Zhou, Z.Y., Xu, C.H., Zhang, Q.L., 2008. Geochemical characteristics of Pengchong complex in Longmen Mountain, western Sichuan: petrogenesis and tectonic implications. *Geotecton. Metallog.* 32 (1), 105–116 (in Chinese with English abstract).
- Zhang, R., Sun, Y., Zhang, X., Ao, W., Santosh, M., 2016. Neoproterozoic magmatic events in the South Qinling Belt, China: implications for amalgamation and breakup of the Rodinia supercontinent. *Gondwana Res.* 30, 6–23. <https://doi.org/10.1016/j.gr.2015.06.015>.
- Zhang, S.B., Zheng, Y.F., 2011. On the origin of low $\delta^{18}\text{O}$ magmatic rocks. *Acta Petrol. Sin.* 27, 520–530 (in Chinese with English Abstract).
- Zhao, G.C., Guo, J.H., 2012. Precambrian geology of China: preface. *Precambrian Res.* 222–223, 1–12. <https://doi.org/10.1016/j.precamres.2012.09.017>.
- Zhao, G.C., Cawood, P.A., Wilde, S.A., Sun, M., 2002. Review of global 2.1–1.8 Ga orogens: implications for a pre-Rodinia supercontinent. *Earth-Sci. Rev.* 59 (1–4), 125–162. [https://doi.org/10.1016/S0012-8252\(02\)00073-9](https://doi.org/10.1016/S0012-8252(02)00073-9).
- Zhao, G.C., Wang, Y.J., Huang, B.C., Dong, Y.P., Li, S., Zhang, G.W., Yu, S., 2018. Geological reconstructions of the East Asian blocks: from the breakup of Rodinia to the assembly of Pangea. *Earth Sci. Rev.* 186, 262–286. <https://doi.org/10.1016/j.earscirev.2018.10.003>.
- Zhao, J.H., Zhou, M.F., 2007. Geochemistry of Neoproterozoic mafic intrusions in the Panzhihua district (Sichuan Province, SW China): implications for subduction-related metasomatism in the upper mantle. *Precambrian Res.* 152 (1), 27–47. <https://doi.org/10.1016/j.precamres.2006.09.002>.
- Zhao, J.H., Zhou, M.F., 2008. Neoproterozoic adakitic suite at the northwestern margin of the Yangtze Block, China: evidence for partial melting of thickened lower crust and secular crustal evolution. *Lithos* 104, 231–248. <https://doi.org/10.1016/j.lithos.2007.12.009>.
- Zhao, J.H., Zhou, M.F., 2009. Secular evolution of the Neoproterozoic lithospheric mantle underneath the northern margin of the Yangtze Block, South China. *Lithos* 107, 152–168.
- Zhao, J.H., Zhou, M.F., Yan, D.P., Yang, Y.H., Sun, M., 2008. Zircon Lu-Hf isotopic constraints on Neoproterozoic subduction-related crustal growth along the western margin of the Yangtze Block, South China. *Precambrian Res.* 163 (3–4), 189–209. <https://doi.org/10.1016/j.precamres.2007.11.003>.
- Zhao, J.H., Zhou, M.F., Zheng, J.P., Fang, S.M., 2010. Neoproterozoic crustal growth and reworking of the Northwestern Yangtze Block Constraints from the Xixiang dioritic intrusion, South China. *Lithos* 120, 439–452.
- Zhao, J.H., Zhou, M.F., Yan, D.P., Yang, Y.H., Sun, M., 2011. Reappraisal of the ages of Neoproterozoic strata in South China: no connection with the Grenvillian orogeny. *Geology* 39 (4), 299–302. <https://doi.org/10.1130/G31701.1>.
- Zhao, J.H., Zhou, M.F., Zheng, J.P., 2013. Constraints from zircon U-Pb ages, O and Hf isotopic compositions on the origin of Neoproterozoic peraluminous granitoids from the Jiangnan Fold Belt, South China. *Contrib. Mineral. Petrol.* 166, 1505–1519.
- Zhao, J.H., Asimow, P.D., Zhou, M.F., Zhang, J., Yan, D.P., Zheng, J.P., 2017. An Andean-type arc system in Rodinia constrained by the Neoproterozoic Shimian ophiolite in South China. *Precambrian Res.* 296, 93–111.
- Zhao, J.X., Chen, Y.L., Li, Z.H., 2006. Zircon SHRIMP U-Pb dating of the Kangding complex and its geological significance. *Geosci.* 20 (3), 378–385 (in Chinese with English abstract).
- Zheng, Y.F., Fu, B., Gong, B., Li, L., 2003. Stable isotope geochemistry of ultra-high pressure metamorphic rocks from the Dabie-Sulu orogen in China: implications for geodynamics and fluid regime. *Earth-Sci. Rev.* 62, 105–161.
- Zheng, Y.F., Zhang, S.B., Zhao, Z.F., Wu, Y.B., Li, X.H., Li, Z.X., Wu, F.Y., 2007. Contrasting zircon Hf and O isotopes in the two episodes of Neoproterozoic granitoids in South China: Implications for growth and reworking of continental crust. *Lithos* 96, 127–150.
- Zhou, M.F., Yan, D.P., Kennedy, A.K., Li, Y., Ding, J., 2002. SHRIMP U-Pb zircon geochronological and geochemical evidence for Neoproterozoic arc-magmatism along the western margin of the Yangtze Block, South China. *Earth Planet. Sci. Lett.* 196 (1–2), 51–67. [https://doi.org/10.1016/S0012-821X\(01\)00595-7](https://doi.org/10.1016/S0012-821X(01)00595-7).
- Zhou, M.F., Yan, D.P., Wang, C.L., Qi, L., Kennedy, A., 2006. Subduction-related origin of the 750 Ma Xuelongba adakitic complex (Sichuan Province, China): implications for the tectonic setting of the giant Neoproterozoic magmatic event in South China. *Earth Planet. Sci. Lett.* 248 (1–2), 286–300. <https://doi.org/10.1016/j.epsl.2006.05.032>.
- Zhu, W.G., Deng, H.L., Liu, B.G., Li, Y.C., Qin, Y., Luo, Y.N., 2004. Age of formation of the Mg-Fe-Mg-Fe-Mg complex in the Gaojia Village, Yanbian, Sichuan: the chronological constraints of the U-Pb single-particle zircon and $^{40}\text{Ar}/^{39}\text{Ar}$ of the hornblende. *Chin. Sci. Bull.* 49 (10), 985–992 (in Chinese with English abstract).
- Zhu, W.G., Zhong, H., Li, X.H., Deng, H.L., He, D.F., Wu, K.W., Bai, Z.J., 2008. SHRIMP zircon U-Pb geochronology, elemental, and Nd isotopic geochemistry of the Neoproterozoic mafic dykes in the Yanbian area, SW China. *Precambrian Res.* 164 (1–2), 66–85. <https://doi.org/10.1016/j.precamres.2008.03.006>.
- Zhu, X., Long, X.P., Yang, X.X., Wang, J.Y., 2018. The formation temperature of Neoproterozoic magmatic intrusions in the Hannan area and its geological significance. *Chin. J. Geol.* 53, 1000–1026 (in Chinese with English abstract).
- Zhu, X.Y., Chen, F.K., Liu, B.X., Zhang, H., Zhai, M.G., 2014. Geochemistry and zircon ages of mafic dikes in the South Qinling, central China: evidence for late Neoproterozoic continental rifting in the northern Yangtze block. *Int. J. Earth Sci. (Geol. Rundsch.)* 104, 27–44.
- Zhuo, J., Jiang, Z., Jiang, X., Wang, J., Cai, J., Xiong, G., Lu, J., Cui, X., Liu, J., 2017. SHRIMP Zircon U-Pb Ages for the Stratotype Section of Neoproterozoic Suxiong Formation in Western Sichuan Province and Their Geological Significance. *Geol. Rev.* 63, 177–188 (in Chinese with English abstract).